Lithos 154 (2012) 374–391

Contents lists available at SciVerse ScienceDirect

Lithos

journal homepage: www.elsevier.com/locate/lithos

Petrogenesis and magmatic–hydrothermal evolution time limitation of Kelumute No. 112 pegmatite in Altay, Northwestern China: Evidence from zircon U–Pb and Hf isotopes

Zheng-Hang Lv [a,b], Hui Zhang [a,*], Yong Tang [a], Shen-Jin Guan [a,c]

[a] Laboratory for High Temperature & High Pressure Study of the Earth's Interior , Institute of Geochemistry, Chinese Academy of Sciences, Guiyang 550002, China
[b] Graduate University of Chinese Academy of Sciences, Beijing 100049, China
[c] State Key Laboratory for Mineral Deposits Research and Department of Earth Sciences, Nanjing University, Nanjing 210093, China

ARTICLE INFO

Article history:
Received 10 March 2012
Accepted 4 August 2012
Available online 13 August 2012

Keywords:
Magmatic–hydrothermal evolution
Zircon U–Pb age
Hf isotope
Pegmatite
Granite
Altay, Xinjiang

ABSTRACT

Granitic pegmatites and associated rare-metal deposits, unique features in the Altay orogen, are located in a key tectonic position of the southern Central Asian Orogenic Belt (CAOB) and document the tectonic evolution of the Paleo-Asian Ocean. The Kelumute No. 112 pegmatite, which intruded into the Jideke two-mica granites, hosts abundant rare-metal (e.g., Li, Be, Nb, Ta) ore deposits and ranks only second to the Koktokay No. 3 pegmatite in both size and reserves. To explore the evolution time limitation of magmatic, magmatic–hydrothermal and hydrothermal stages in the pegmatite magma system, the tectonic setting and the genetic relationship between pegmatites and granites, this study presents zircon U–Pb and Hf isotopic compositions of the Kelumute No. 112 pegmatite and the wall rocks (two-mica granite and biotite granite) as determined by LA-ICPMS and LA-MC-ICPMS. The weighted mean $^{206}Pb/^{238}U$ ages of the internal textural zones of the pegmatite, including zones I, II, III, V and VI, are 238.3 ± 2.0 Ma, 233.5 ± 3.7 Ma, 188.3 ± 1.7 Ma, 218.8 ± 1.9 Ma and 210.7 ± 1.6 Ma, respectively. Wall rocks of two-mica granite and biotite granite are dated at 445.6 ± 4.3 Ma and 455.6 ± 5.4 Ma, respectively. Zircons from the Kelumute No. 112 pegmatite have lower positive $\varepsilon_{Hf}(t)$ values (+0.03 to +2.35), with T_{DM} model ages of 1112–1225 Ma. Wall rocks show similar zircon $\varepsilon_{Hf}(t)$ values (−1.41 to +4.13) and T_{DM} model ages (1172 to 1515 Ma). However, three xenocrystic zircons from the granites are characterized by larger negative εHf(t) values (−5.85 to −9.83) and older T_{DM} model ages (1839 to 2090 Ma). Thus, the following conclusions can be drawn: 1) the Kelumute No. 112 pegmatite and its wall rocks (Jideke two-mica granite and biotite granite) have no genetic relationship, as indicated by the large gaps between their formation ages. However, they did originate from a common source composed of ancient crust and mantle-derived materials under two different tectonic settings; 2) the magmatic, magmatic–hydrothermal transition and hydrothermal stages of the No. 112 pegmatite magma lasted for ~5 Ma, ~23 Ma and ~22 Ma, respectively; and 3) the No. 112 pegmatite magma was most likely formed in a post-collision tectonic setting, indicating that block amalgamation and collisional orogeny of the CAOB continued into the Triassic.

1. Introduction

The Central Asia Orogenic Belt (CAOB, also called the Altaids, or the Central Asia Fold Belt) is known as one of the largest Phanerozoic accretionary orogenic belts in the world (Yuan et al., 2007a; Xiao et al., 2008a) and is situated between the Siberian craton to the North and Tarim and the North China craton to the South (Fig. 1). It is now widely accepted that the tectonic evolution of the CAOB is dominated by the complicated accretion–collision of arcs, accretionary complexes, oceanic plateaus and seamounts (Buslov et al., 2001; Coleman, 1989), Precambrian micro-continents, island arcs, and ophiolites (Kröner et al., 2007; Windley et al., 2007; Xiao et al., 2004, 2008b, 2009) during the evolution of the Paleo-Asian Ocean from the Late Precambrian to the Mesozoic. Its prolonged and complicated orogenic process gave rise to formation of multiple types of world-class ore deposits including gold, silver, copper–molybdenum, nickel, lead–zinc and rare-metal, known as "the Central Asian Metallogenic Domain" (Zhu, 2007). Magmatic, metamorphic and relevant metallogenic events in this orogenic belt are a record that provides valuable information on the origin and evolution of the CAOB, but progress in unraveling its tectonic history has been retarded by a lack of reliable age data (Yuan et al., 2007a) and detailed studies of this vast area. Therefore, the time and mechanism of the final formation of the CAOB remains controversial (Xiao et al., 2009) and the final closure time of the Paleo-Asian Ocean is not clear: previous studies

* Corresponding author. Tel.: +86 851 5891494; fax: +86 851 5895161.
E-mail address: zhanghui@vip.gyig.ac.cn (H. Zhang).

0024-4937/$ – see front matter © 2012 Elsevier B.V. All rights reserved.
http://dx.doi.org/10.1016/j.lithos.2012.08.005

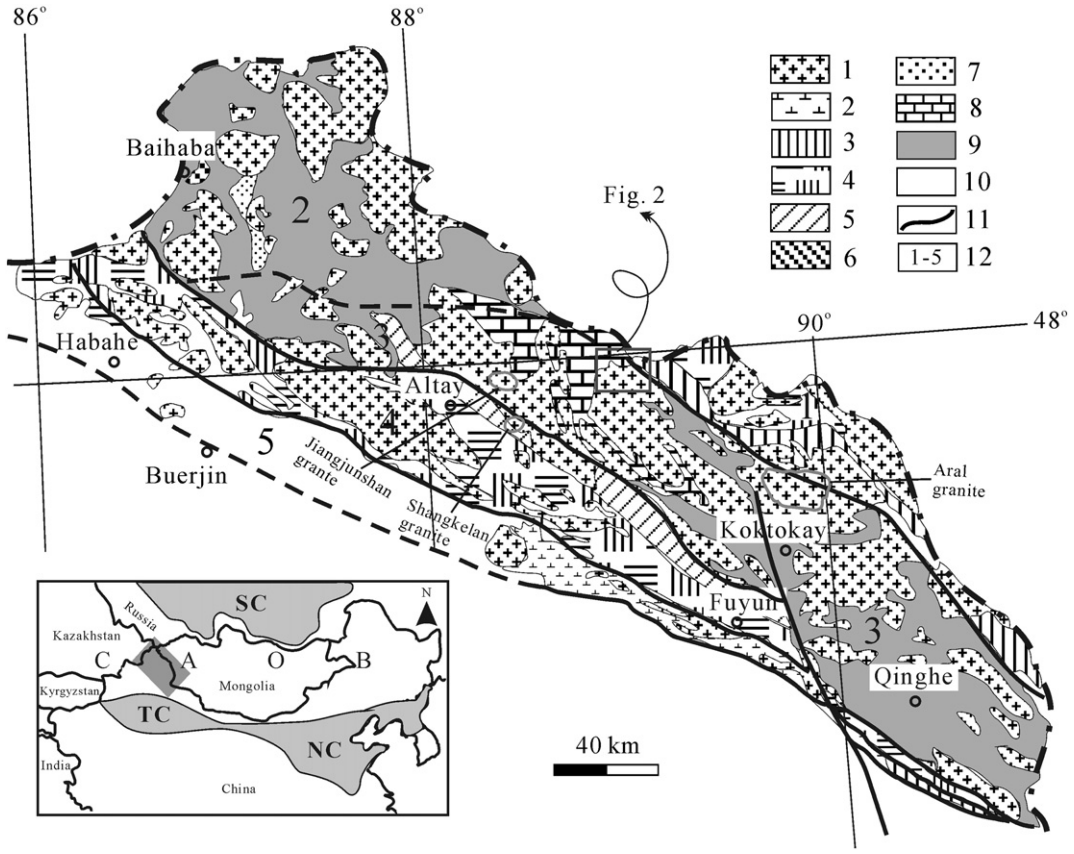

Fig 1. Geological sketch map of the Chinese Altay, showing the tectonic setting of the Kelumute No.112 pegmatite (modified from He et al., 1990; Li et al., 1996; Windley et al., 2002). Abbreviation: CAOB = Central Asian Orogenic Belt; SC = Siberia Craton; TC = Tarim Craton; NC = North China Craton. 1, granite; 2, undivided gneiss; 3, Carboniferous; 4, Altay Formation; 5, Kangbutiebao Formation; 6, Bahaba Formation; 7, Dongxilieke Formation; 8, Kulumuti Group; 9, Habahe Group; 10, Cenozoic sedimentary; 11, Fault; 12, Terrane numbers.

have proposed the Ordovician–Silurian (He et al., 1994; Kheraskova et al., 2003), Devonian–Carboniferous (Hendrix et al., 1996; Safonova et al., 2004), and Carboniferous–Permian (Buslov et al., 2004; Filippova et al., 2001; Li et al., 2003; Wang et al., 2010; Xu et al., 2001; Zhang et al., 2003). Recently, the argument has primarily focused on the Late Carboniferous (Chen et al., 2010; Han et al., 2010, 2011) and Permian–Triassic (Briggs et al., 2007; Xiao et al., 2006, 2008b, 2009, 2010). Although many reports have studied the evolution of the CAOB in terms of pre- to syn-orogenic records such as ophiolites, volcanic rocks and granites, the topic is still under debate.

An important part of the CAOB, the Chinese Altay has great potential for the exploitation of precious metals (Au, Ag), non-ferrous metals (Cu, Mo, Pb, Zn,), rare metals (Li, Be, Nb, Ta), iron ore and non-metallic mineral products such as gems and muscovite. The Chinese Altay was in a passive continental margin from the late Precambrian to the early Paleozoic, before orogenic movement began (Chen et al., 1999), at which point its tectonic setting changed to a continental magmatic arc (active continental margin) during the middle Cambrian to Ordovician (Windley et al., 2002), Middle Cambrian to late Devonian (Wang et al., 2006), and early Cambrian to late Carboniferous (Cai et al., 2011a,c). The corresponding subduction and accretion processes began at ca. 460 Ma and culminated at ca. 408 Ma, resulting in a generation of plentiful Early–Middle Paleozoic granites (Liu et al., 2008a; Cai et al., 2011a,b,c; Yuan et al., 2007a; Sun et al., 2008; Tong et al., 2005; Wang et al., 2005, 2006; Windley et al., 2002; Yuan et al., 2006). An extensional setting in a back-arc basin began during the Devonian–early Carboniferous, according to studies of bimodal volcanic rocks (407 Ma, Zhang et al., 2000), gabbro (405 Ma, Wang et al., 2006) and ophiolite (372 to 352 Ma, Wu et al., 2006; Xu et al., 2003; Zhang et al., 2003). Some scholars have proposed an extensional forearc setting during the Devonian, Late Carboniferous, and Permian (Yuan et al., 2007a). It was thus concluded that the Altay orogenic belt was mainly built up during the early–middle Paleozoic (500 to 380 Ma) (Wang et al., 2006; Windley et al., 2002). Late Paleozoic granites have also been reported systematically (Tong et al., 2006a,b, 2007, 2012), suggesting vertical growth (2.1 to 1.5%) of the continental crust in the Chinese Altay (Tong, 2006). The Mesozoic magmatism from this region appears to contribute very little (Chen et al., 1999; D.H. Wang et al., 2003; Wang et al., 2000; Zhang et al., 1994), but increasing numbers of granite and granitic pegmatite have been reported in recent years (Chen, 2011; Ren et al., 2011; Wang et al., 2007, 2010; Zhu et al., 2006). Previous work suggested that the Chinese Altay has mainly undergone three orogenic stages, including the syn-orogenic (460 to 380 Ma), post-orogenic (290 to 260 Ma) and anorogenic stage (after the end-Permian) (He et al., 1994; Hu et al., 2000; Li et al., 2003; Wang et al., 2005, 2010; Windley et al., 2002; Xiao et al., 2004; Xu et al., 2001).

Granitic pegmatite and associated rare-metal deposits are widely exposed in the Chinese Altay. According to previous work, there are nearly one hundred thousand pegmatite veins in a ~20,000 km^2 area (including the Rudny Altay and Gobi Altay) (Wu and Zou, 1989). As one type of independent deposit, pegmatites are enormously economically valuable in rare metal exploitation and are also excellent indicators of tectonic evolution (D.H. Wang et al., 2004b; Wang et al., 2002). Previous studies of the Altay pegmatites have mainly focused on the mineralogy, diagenesis and evolution of pegmatite (Lu et al., 1996; Wu and Zhu, 1995; Wang and Zou, 1981; Wu et al., 1994; Zhang, 2001; Zhang and Liu, 2001; Zhang et al., 2004; Zhu et al., 2000); little is known about the formation ages, provenance and tectonic settings of pegmatites in this

belt. As a result, its importance in the tectonic evolution of the CAOB is not clear.

The Kelumute No. 112 pegmatite, which intrudes into the Jideke two-mica granite, hosts a large-scale rare metal (Li–Be–Nb–Ta) ore deposit and ranks only second to the well-known Koktokay No. 3 pegmatite in Xinjiang, NW China. To date, its emplacement age, metallogenic epoch, the evolution time-scale of its magmatic–hydrothermal system, the formation age of wall rocks, provenance, and the genetic relationship between the pegmatite and wall rocks remain unclear. In this paper, a systematic study of zircon U–Pb chronology and Hf isotopic composition of the five internal textural zones from the pegmatite and two granite samples from the wall rocks was carried out using LA-ICPMS and LA-MC-ICPMS, respectively, to (1) investigate the formation and evolution of the pegmatite; (2) determine the genetic relationship between the pegmatite and two-mica granite; (3) define the evolution time-scale of magmatic, magmatic–hydrothermal and hydrothermal stages in natural pegmatitic magma; and (4) reveal the original tectonic setting of the No. 112 pegmatite magma.

2. Geological descriptions

2.1. Regional geology

The Altay orogenic belt, a major part of the CAOB, extends from Eastern Kazakhstan, Russia through Northwest China to Southern Mongolia. It is situated between the Sayan to the north and Kazakhstan–Junggar block to the south (Windley et al., 2002; Xiao et al., 1992, 2004). The Chinese Altay region was divided into five fault-bounded terranes on the basis of stratigraphy, metamorphism, deformation pattern, magmatic activity and geochronology (Fig. 1). Recently, a four-domain scheme has been widely accepted (Yuan et al., 2007a; Cai et al., 2011a; Sun et al., 2008), comprising the north domain (Unit 1 in Fig. 1), the central domain (Unit 2 and 3 in Fig. 1), the Qiongkuer domain (Unit 4 in Fig. 1) and the south domain (Unit 5 in Fig. 1). The north Altay domain mainly consists of the Devonian to Early Carboniferous metavolcanic (andesite and dacite) and metasedimentary rocks, which are intruded upon by undeformed biotite granitic plutons. The central domain makes up an important part of the Altay microcontinent, including Unit 2, which predominantly consists of a thick Neoproterozoic to middle Ordovician–early Devonian turbiditic and pyroclastic sequence (Habahe Group), and Unit 3, which contains amphibolite- and greenschist facies metasediments and volcanics. Widespread granitic batholiths, abundant pegmatites with rare-metal mineralization and a few mafic–ultramafic stocks developed in this domain. According to geochemical data from the Habahe Group and zircon U–Pb age data, a Proterozoic basement most likely existed (Hu et al., 2000; Li et al., 2006; Sun et al., 2008; Tong et al., 2006a,b). The Qiongkuer domain consists mainly of late Silurian sedimentary rocks (Kulumuti Group) and early Devonian arc-related pyroclastic rocks (Kangbutiebao Formation) in the lower part and a middle Devonian turbiditic sand–shale sequence (Altai Formation) in the upper part, with a metamorphic grade from greenschist to upper amphibolite facies. The south domain is mainly composed of Devonian fossiliferous successions that are, in turn, overlaid with late Carboniferous formations. Gneisses and schists also occur locally. Further south, the Chinese Altai is separated from the Junggar block by the Erqis Fault, a large-scale (1000 km) sinistral strike-slip fault in central Asia (Fig. 1) (Cai et al., 2011b; He et al., 1990; Hu et al., 2000; Wang et al., 2007; Windley et al., 2002).

2.2. Geology of the mining area

The Kelumute mining area is located in northern Altay in the Xinjiang Uygur Autonomous Region, close to the border between China and Mongolia and approximately 147 km from the city of Altay. This pegmatite concentration area was identified in the Kelumute–Kukalagai rare-metal and muscovite metallogenic sub-belt of the Qinghe–Halong metallogenic belt. The mining area lies on the northwestern Kelumute–Jideke orefield (approximately 7.5 km^2), adjacent to the northeast limb of the Baliersi–Kayierti fold belt, north of the middle part of the Kurekete–Kumualashan fault, and east of the Kuermutu–Mangdaiqia fold belt. It consists largely of Paleozoic metamorphic rock and large-scale intermediate-acid rock (Fig. 2). The Upper Habahe subgroup sporadically crops out on both sides of the Kelumute River with small-scale outcrops (500 m × 125 m at the most) and is composed of biotite–quartz schist and banded migmatite. Magmatic rocks developed well and make up 95% of the whole mining area, including fine-grained gneissic two-mica granite, underlying biotite granite and peripheral granodiorite. The Kelumute No. 112 pegmatite directly intruded into the gneissic two-mica granite, which is downstream of the Kelumute stock. The biotite granite and granodiorite belong to the midstream of the Baliersi stock. Field investigations demonstrate that two-mica granite intruded into the biotite granite in an abrupt interface. Four sets of faults were identified in the mining area, with the strikes of EW, NW, NE and SN. The first two are ore-capacity faults filled by pegmatites hundreds to thousands of meters in length and several to dozens of meters in width; the latter two are smaller post-metallogenic faults less than one hundred meters in length and less than ten meters in width.

2.3. Geological features of No. 112 pegmatite

The No. 112 pegmatite, a LCT-type (Li, Rb, Cs, Be, Ga, Sn, Nb<Ta, B, P, F) pegmatite according to the classification by Černý (1991), Černý and Erict (2005), intruded into the gneissic two-mica granite. The pegmatite vein has an S-shape 1,380 m in length and 3 to 12 m in width. As cut by two "block streams," it was divided into eastern, middle and western sections, with strikes of NW, N and NE, and dip angles of 40°, 50° and 45°, respectively (Fig. 3). The mineralization grades are different for all three sections: richest in the middle section and poorest in the west section. The western section is bed- or wedge-like: 280 m in length with horizontal thickness varying from 2.5 m (east) to 4 m (west). The middle part, hosting the best and largest ore body of the No. 112 pegmatite, is bed-like: approximately 660 m in length and 7 m in width. The eastern section is also bed-like: 440 m in length and 5.5 m in width

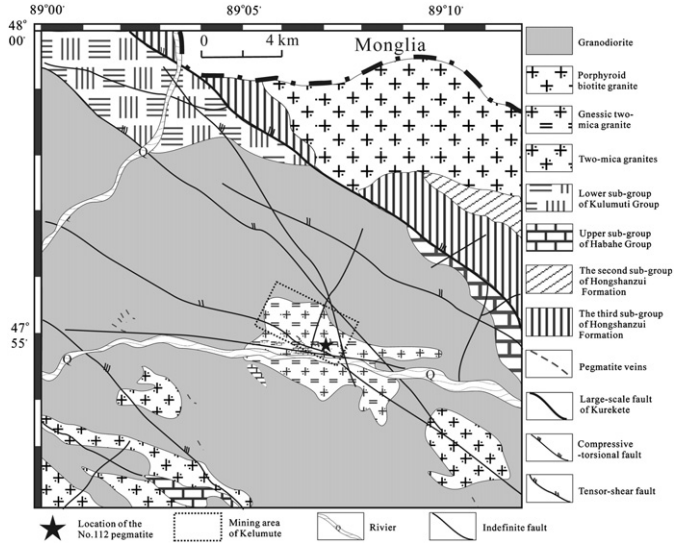

Fig. 2. Geological map of Kelumute–Jideke pegmatite filed, showing the occurrence of the Kelumute No.112 pegmatite.

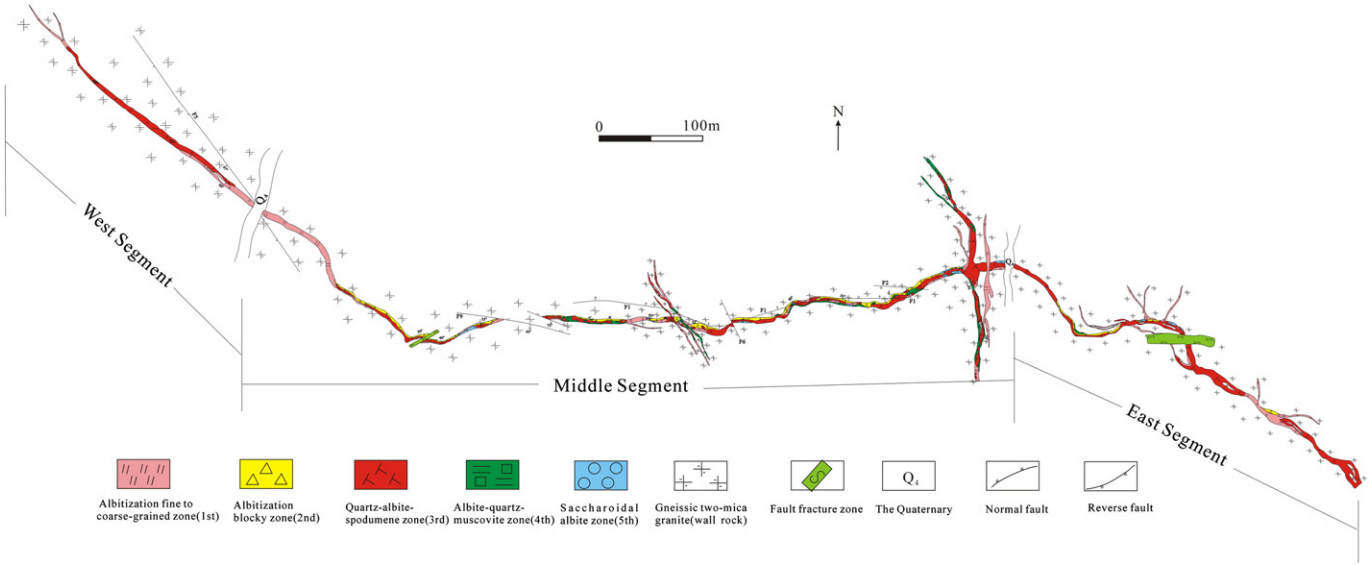

Fig. 3. Geological map of textural zones of the Kelumute No.112 pegmatite. Five main textural zones including: medium fine-medium coarse grained albitization (zone I); small blocky albitization (zone II); quartz–albite–spodumene (zone III); albite–quartz–muscovite (zone IV); saccharoidal albite (zone V). Country rock is gneissic two mica granite.

on average. Based on mineral associations, the No. 112 pegmatite was divided into the following six textural zones:

Zone I (albitization fine- to coarse-grained zone), which accounts for 20 vol.% of the No. 112 pegmatite. Main rock-forming minerals include quartz (30%), microcline (28%), albite (37%) and muscovite (2–3%). It develops along the hanging wall and footwall and appears as continuous bands 10–15 m in length and 0.3–2 m in width.

Zone II (albitization blocky zone) is approximately 5 vol.% of the pegmatite and is composed of quartz (25%), microcline (45–60%), albite (10–15%) and muscovite (1–2%). It has a nest-like or banding distribution along the hanging wall, commonly 5–10 m in length and 1–3 m in width.

Zone III (quartz–albite–spodumene zone) accounts for 60 vol.% of the pegmatite and mainly includes rock-forming minerals including quartz (30%), albite (35%), spodumene (25–30%), microcline (5%) and muscovite (3%). It appears as continuous bands and develops on the middle zone or along the hanging wall and footwall of the vein, with a length of 20–50 m and a width of 3–5 m.

Zone IV (albite–quartz–muscovite zone) accounts for 2 vol.% of the pegmatite and is mainly composed of quartz (30%), albite (25%), muscovite (20%) and microcline (15–20%). It appears as small nests or vein-like formations, sporadically hosted in zones I, II, and III, usually with a length of 5–10 m and a width of only tens of centimeters.

Zone V (saccharoidal albite zone) makes up 13 vol.% of the No. 112 pegmatite and is composed of albite (86%), quartz (10%) and muscovite (2%). It develops as single, cluster or nest-like formations that are generally 3–8 m in length and 0.5–2 m in width.

Zone VI (quartz core zone) is only a very small proportion (<1 vol.%) of the pegmatite vein and is mainly composed of quartz (>95%), with very little albite and muscovite. It appears as nest-like formations and is randomly distributed in the middle zone of the vein.

3. Samples and analytical methods

After a halt in production of the Kelumute No. 112 pegmatite rare-metal ore deposit in the 1990s, the mining tunnel was subsequently closed. All pegmatite samples were picked from the ore sample storeroom rather than from outcrops, based on the mineral associations of the six textural zones. To meet the requirement for zircon quality and quantity, all pegmatite samples were fresh and of sufficient mass (>10 kg). Two granite samples (approximately 4 kg) were collected from the outcrop close to the pegmatite. All samples were pulverized by hand-grinding in a stainless steel mortar and pestle and screened through a sieve with a mesh size of 380 μm (pegmatite) or 250 μm (granite). Zircon grains were concentrated by flotation and magnetic separation, and the individual zircon grains were finally handpicked under a binocular microscope. Zircon target preparation, image acquisition under reflected light and cathodoluminescence (CL), and in situ U–Pb analyses using laser ablation inductively coupled plasma mass spectrometry (LA-ICPMS) were carried out in the State Key Laboratory of Continental Dynamics, Department of Geology at Northwest University, Xi'an. The laser-ablation system was a GeoLas 200 M (Lambda Physik and MicroLas, Germany) equipped with an Agilent7500a ICP-MS. The conditions were as follows: laser frequency of 10 Hz with an energy of 34–40 mJ, beam diameter of 30 μm, ablation depth of 20–40 μm, background acquisition of 30 s and signal acquisition of 60 s. Helium was used as a carrier gas to enhance the transport efficiency of the ablated materials (Yuan et al., 2007b). Zircon 91500 was used as an external standard to normalize isotopic discrimination, and ^{29}Si and NIST610 were used as internal standards to calibrate and normalize the concentrations of U, Th and Pb, respectively. Isotopic ratios of U–Th–Pb were calculated using ICPMS Data Cal (Liu et al., 2008b; Liu et al., 2010), and the apparent and Discordia U–Pb ages were calculated using the ISOPLOT program (Ludwig, 2003). Correction of common Pb was achieved according to the method of Andersen (2002). The uncertainty of individual analyses is reported with 1σ and the weighted mean ^{206}Pb/^{238}U age was calculated at the 2σ level.

Zircon Hf isotopic analysis was carried out using a Nu plasma multi-collector ICPMS equipped with a UP-213 laser-ablation system (LA–MC-ICPMS) at the State Key Laboratory of Environmental Geochemistry, Institute of Geochemistry, Chinese Academy of Sciences. The zircon analyses were conducted with a beam diameter of 60 μm, 5 Hz (hafnian zircons from pegmatites) and 10 Hz (ordinary zircons from granites) repetition rate. Laser beam energy density was 4.40–5.27 (hafnian zircons) and 5.27–6.15 J/cm^2 (ordinary zircons). The detailed instrumental settings and analytical procedures were described by Tang et al. (2008). The determined ^{176}Hf/^{177}Hf ratios of 0.282309 ± 0.000021 (2σ, n = 25) for zircon standards 91500 were in good agreement with the reported values (Woodhead et al., 2004).

4. Results

4.1. Th/U ratio and CL feature of zircon

Sample KLP-1 from zone I: zircon grains varied in size from 200 to 450 μm, and in color from brown to dark brown with opaque, euhedral tetragonal-dipyramid or stubby tetragonal prism shapes. Zircons showed taxitic and mottled textures with weak cathodoluminescence (CL). Most displayed faint, weakened remnants of the original oscillatory zoning on their mantles and rims but showed no evidence of concentric zones in their cores. A certain amount of poikilitic mineral inclusions are randomly hosted in zircons (Fig. 4a). These characteristics indicate that zircons from zone I were magmatic in origin but suffered from metamictization after crystallization due to high U and Th content and lower-grade recrystallization during interaction with the deuteric fluid. Some analytical spots showed extreme high U (13,777 ppm in spot 1.14 and 16,834 ppm in spot 1.15) or Th (10,838 ppm in spot 1.3) content, while other spots showed relatively low U and Th content (Table 1), varying from 2669 to 9882 ppm U and 302 to 7752 ppm Th. The Th/U ratios of all 14 spots ranged from 0.04 to 1.35.

Sample KLP-2 from zone II: zircon grains varied in size from 250 to 500 μm and were brown, translucent or opaque, with a euhedral tetragonal-dipyramid or stubby tetragonal prism shape. Most zircons displayed translucent rims under reflected light and weakened oscillatory zoning with intense cathodoluminescence (CL), indicating magmatic origin and low-grade recrystallization (spots 2.5, 2.12 and 2.14, Fig. 4b). The mantles and cores of these zircons usually displayed a porous, spongy texture with few blurred remnants of the original oscillatory zoning (spots 2.6 and 2.3), which provide evidence for patchy recrystallization in the presence of fluid. Some zircon rims developed microfractures owing to radioactive damage from high U and Th content in the mantles and cores. The porous, spongy area of the zircons was characterized by extremely high U content (i.e., 10,536 ppm and 17,568 ppm U in spot 2.6 and spot 2.16), indicating a significant influence from metamictation. These two spots aside, the U and Th contents of other analytical spots ranged from 801 to 6420 ppm and 13 to 1279 ppm, respectively, with Th/U ratios of 0.01 to 0.13 (Table 1).

Sample KLP-3 from zone III: zircon grains ranged in size from 200 to 400 μm and were dark brown and opaque, with a subhedral tetragonal-dipyramid or euhedral stubby tetragonal prism shape. Almost all zircons displayed weak CL and no concentric oscillatory zones. Some exhibited dim but homogenous areas coexisting with small recrystallized areas (spot 3.12, Fig. 4C), indicating that recrystallization happened over a limited range, while other zircons displayed a taxitic or mottled texture (spots 3.10 and 3.15). Due to the high content of U (from 1687 ppm to 23,639 ppm) and Th (from 55 ppm to 4294 ppm) (Table 1), these zircons experienced metamictization and/or recrystallization in the presence of fluid, with a lower grade than that of zones I and II. The Th/U ratios of zircons in KLP-3 normally varied from 0.01 to 0.48.

Sample KLP-5 from zone V: zircon grains are 100–300 μm in size, gray and translucent, with a subhedral tetragonal-dipyramid or euhedral stubby tetragonal prism shape. Zircon CL images are characterized by a striking contrast between bright and dark areas, and the dark areas are homogenous with (Fig. 4d, spots 5.7, 5.16) or without (spot 5.13) oscillatory zoning, which is regarded as a remnant of primary zircons. The light areas show blurred remnants of the original oscillatory zoning (spot 5.9) and a spotted texture (spot 5.10) or a homogenous composition (spot 5.18) resulting from recrystallization of primary zircons of different grades. Comparison with zircons from zones I, II and III shows a higher-grade recrystallization. Recrystallized zircon areas are characterized by lower U (111–298 ppm) and Th (5–20 ppm) content, with Th/U ratios ranging from 0.02 to 0.14 (only one ratio was greater than 0.1, Table 1). However, the remnants of primary zircons exhibited higher U (316–7085 ppm) and Th (27–371 ppm) content, with Th/U ratios in the range of 0.01 to 0.11.

Sample KLP-6 from zone VI: zircon grains with sizes of 150–350 μm, dark brown and translucent, with a subhedral tetragonal-dipyramid or euhedral stubby tetragonal prism shape. CL images display a metasomatic relict texture in zircons, indicating that they suffered from intensive metasomatic alteration and that the remnant primary rims (Fig. 4e, left zircons), and other tiny primary areas remained in the mantles and cores with irregular shapes and random distributions. Zircons, which suffered from limited metasomatic alteration, preserve primary areas with weak CL and harbor structures or/and regular shapes and homogenous compositions (Fig. 4e, right zircons) surrounded by blurred and spongy rims. These features indicate that primary zircons suffered from metamictization, metasomatic alteration of fluids, and recrystallization of different grades. Except for extremely high U (10,484 ppm, 27,182 ppm and 22,647 ppm in spots 6.3, 6.5 and 6.9) and Th (2641 ppm, 1042 ppm, 1604 ppm and 1207 ppm in spots 6.5, 6.6, 6.7 and 6.9) content, the zircon content of U and Th in this zone ranged from 16 to 360 ppm and 2206 to 9412 ppm, respectively, with Th/U ratios in the range of 0.01 to 0.26 (Table 1).

KLW-1 (two-mica gneissic granite): zircon grains are 80–200 μm in size, pale yellow and transparent, with a euhedral spindly or stubby tetragonal prism shape. Most zircons show bright CL and clear homogenous areas with no concentric oscillatory zones (Fig. 4f). Th and U content varied from 34 to 380 ppm and 121 to 1022 ppm, respectively, with Th/U ratios from 0.16 to 0.66 (Table 2), indicating that these zircons originated from magma.

KLW-2 (biotite granite): zircon grains were 100–250 μm, yellow and transparent, with a euhedral tetragonal prism shapes. CL images of zircons displayed a clear and periodic zonal texture (Fig. 4g). As Th and U content varied from 39 to 357 ppm and 235 to 637 ppm, with Th/U ratios from 0.09 to 0.78 (Table 1), these zircons are also magmatic in origin.

4.2. Zircon U–Pb geochronology of the Kelumute No. 112 pegmatite

4.2.1. KLP-1

A total of seventeen spots from the cores, mantles and rims of zircons were selected for determination of U and Pb (Table 1). Three (spots 1.9, 1.10 and 1.16, not listed in Table 1) displayed unusually high Th content (6.5% to 8.1%), most likely due to inclusions of thorium-bearing minerals such as thorite and monazite. Fourteen spots evidently deviate from the concordia in the diagram (Fig. 5a), but three spots (spot 1.4, 1.7 and 1.17) yielded three different $^{206}Pb/^{238}U$ ages of 311, 249, and 256 Ma, respectively. The other eleven spots define an extraordinary similar $^{206}Pb/^{238}U$ age population, varying from 237 to 242 Ma. They yield a weighted mean $^{206}Pb/^{238}U$ age of 238.3 ± 2.0 Ma (Fig. 5a), which most likely represents the crystallization age of zircons.

4.2.2. KLP-2

Twenty-one spots for the determination of U and Pb were selected from zircon primary rims and domains that suffered from metamictization, fluid alteration and recrystallization (Table 1). All $^{206}Pb/^{238}U$ ages varied from 102 to 236 Ma, and five spots from the primary rims showed intense CL and clear oscillatory zoning, yielding concordant ages of 229–236 Ma and a weighted mean age of 233.5 ± 3.7 Ma. Two other spots, also from the rims, displayed a weak CL and blurry oscillatory zoning, yielding somewhat concordant ages of 215 and 216 Ma, which indicates overgrowth rims during the magmatic–hydrothermal stage or Pb loss. Seven spots from bright and homogeneous domains in CL yielded ages varying from 179 to 193 Ma and a weighted mean age of 186.3 ± 2.9 Ma, most likely representing the time of complete recrystallization during the hydrothermal stage. The remaining nine spots, which are from the spongy core (spot 2.6) and areas that suffered significant metamictization and/or fluid alteration, yielded younger ages, with less concordance, from 102 to 197 Ma, most likely due to radioactive Pb loss. Therefore, the weighted mean age of

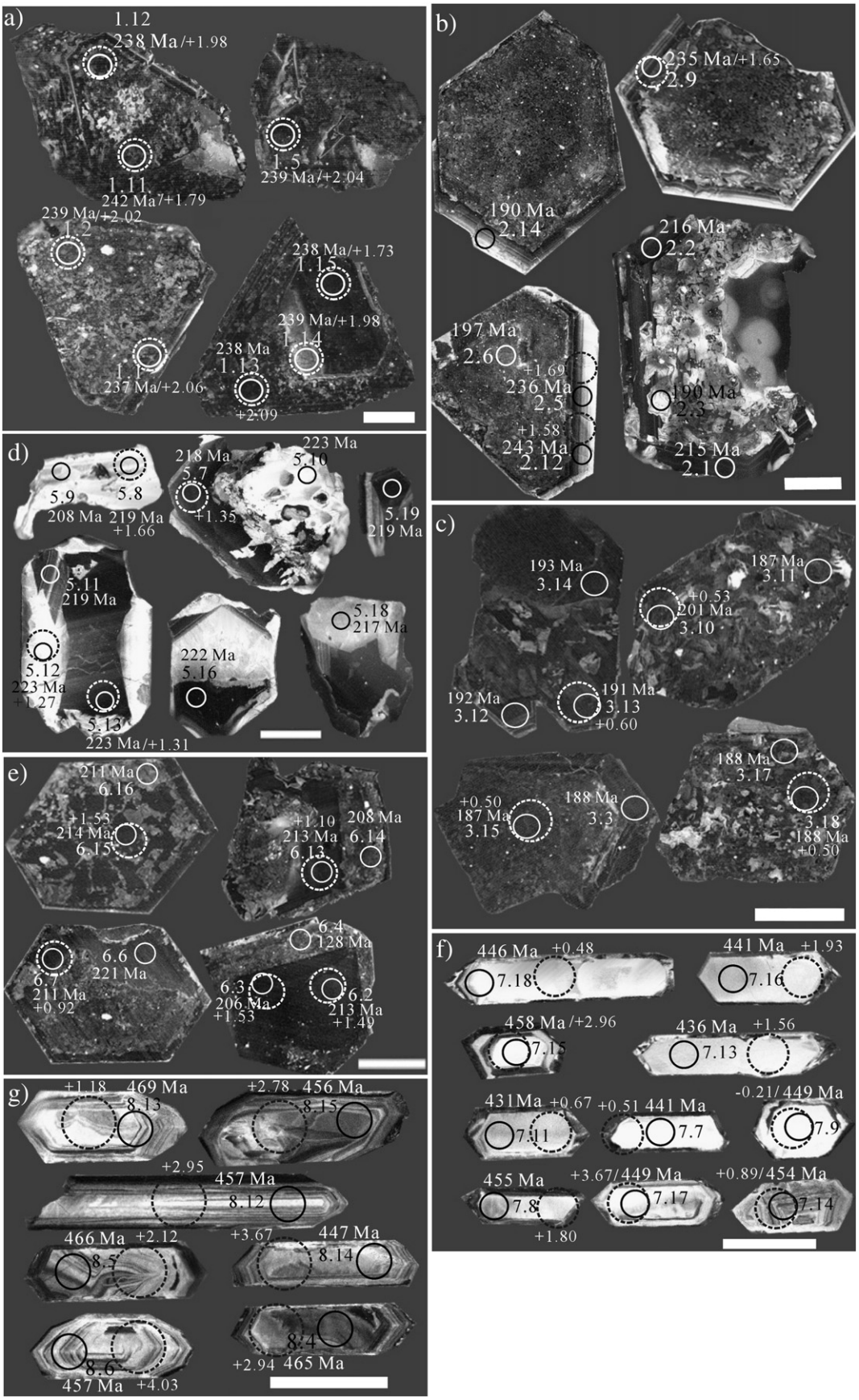

Fig. 4. Representative cathodoluminescence (CL) images, showing the laser analytic spots, $\varepsilon_{Hf}(t)$ values and $^{206}Pb/^{238}U$ ages of zircon grains from Kelumute No.112 pegmatite and wall rocks of granites. (a) sample KLP-1; (b) sample KLP-2; (c) sample KLP-3; (d) sample KLP-5; (e) sample KLP-6; (f) sample KLW-1; (g) sample KLW-2. Scale bars correspond to 100 μm.

233.5 ± 3.7 Ma represents the time when the pristine zircons crystallized.

4.2.3. KLP-3

A total of twenty spots were selected from the cores, mantles and rims of zircons for the determination of zircon U–Pb age. The twenty $^{206}Pb/^{238}U$ ages varied from 159 to 316 Ma (Table 1). Fifteen samples yielded a narrow age range from 172 to 201 Ma, including ten points from dark and homogenous areas that suffered little metamictization and defined an age population with a weighted mean $^{206}Pb/^{238}U$ age of 188.3 ± 1.7 Ma. We considered this age to be the zircon crystallization time (Fig. 5c).

4.2.4. KLP-5

Twenty spots from the remnant primary rims, mantles, cores and recrystallization areas were used to determine U and Pb contents. The twenty $^{206}Pb/^{238}U$ ages varied from 141 to 226 Ma; sixteen of these defined an age population with a weighted mean $^{206}Pb/^{238}U$ age of 218.8 ± 1.9 Ma. The other four points indicated younger ages and deviated from the concordia due to significant radioactive Pb loss. Therefore, we regarded the older age as the time when zircons crystallized (Fig. 5d).

4.2.5. KLP-6

Twenty spots were selected from cores, mantles and rims, and used to determined U and Pb content. The $^{206}Pb/^{238}U$ ages varied from 128 to 267 Ma (Table 1). Thirteen spots, obtained from black primary cores and domains that suffered limited metamictization, contained lower U (2954–10,484 ppm) and Th (16–213 ppm) content, defining an age population varying from 200 to 218 Ma with a weighted mean age of 210.7 ± 1.6 Ma. Four of the remaining spots yielded scattered and meaningless ages (232 to 267 Ma) due to higher content of U (5750–27,182 ppm) and Th (360–2641 ppm). Two spots indicated younger ages (128 and 192 Ma) deviating significantly from the concordia due to Pb loss. One point displayed an unusual Pb/U ratio that may have been due to a feldspar inclusion (not listed in Table 1). Therefore, the weighted mean $^{206}Pb/^{238}U$ age of 210.7 ± 1.6 Ma was considered the crystallization time of zircons (Fig. 5e).

4.3. Zircon U–Pb geochronology of granites

4.3.1. KLW-1

Eighteen spots for the determination of U and Pb were selected from domains of bright CL, homogenous composition and clear oscillatory zoning of zircons. Of these, fifteen yielded an age population with a weighted mean age of 445.6 ± 4.3 Ma, representing the crystallization age of zircons (Fig. 5f). Two spots yield younger ages of 415 and 437 Ma (Table 2, spots 1.2 and 1.4), deviating from the concordia due to a small amount of Pb loss or inclusions. The remaining spot yielded an older concordant age of 509 Ma, most likely representing the formation age of xenocrysts.

4.3.2. KLW-2

Fifteen spots were selected from domains of homogenous composition or clear oscillatory zoning for U–Pb analysis. Thirteen samples yielded an age population with a weighted mean $^{206}Pb/^{238}U$ age of 455.6 ± 5.4 Ma, representing the formation age of the zircons (Fig. 5g). The others defined two older concordant ages of 514 Ma and 498 Ma (Table 2, spots 2.3, 2.11), representing the formation age of xenocrysts.

4.4. Zircon Hf isotopic composition of the Kelumute No. 112 pegmatite

4.4.1. KLP-1

Fifteen spots from twelve zircon grains yielded $^{176}Hf/^{177}Hf$ values from 0.282672 to 0.282688 (Table 3), indicating that the initial $^{176}Hf/^{177}Hf$ ratios were not affected by hydrothermal alteration during the hydrothermal stage. Based on the zircon U–Pb weighted average age of 238 Ma, the calculated $\varepsilon_{Hf}(t)$ values ranged from +1.7 to +2.26, with T_{DM} model ages of 1122 to 1157 Ma.

4.4.2. KLP-2

Fifteen spots displayed nearly the same $^{76}Hf/^{177}Hf$ values, from 0.282660 to 0.282675, except for one higher $^{176}Hf/^{177}Hf$ value of 0.282694 (Table 3). According to the crystallization time of 233 Ma, the calculated $\varepsilon_{Hf}(t)$ values ranged from +1.16 to +2.35, with T_{DM} model ages of 1112 to 1188 Ma.

4.4.3. KLP-3

Fifteen zircon grains yielded $^{176}Hf/^{177}Hf$ values of 0.282656 to 0.282680 (Table 3), and the calculated $\varepsilon_{Hf}(t)$ values varied from +0.03 to +0.88 based on the crystallization time of 188 Ma, with T_{DM} model ages of 1171 to 1225 Ma.

4.4.4. KLP-5

Fifteen zircon grains yielded $^{176}Hf/^{177}Hf$ values ranging from 0.282669 to 0.282693 (Table 3). According to the crystallization time of 219 Ma, the calculated $\varepsilon_{Hf}(t)$ values varied from +1.17 to +2.02, with T_{DM} model ages of 1122 to 1176 Ma.

4.4.5. KLP-6

Fifteen zircon grains yielded $^{176}Hf/^{177}Hf$ values of 0.282664 to 0.282690 (Table 3), and the calculated $\varepsilon_{Hf}(t)$ values varied from +0.92 to +1.82 based on crystallization times of 211 Ma, with T_{DM} model ages of 1133 to 1190 Ma.

4.5. Zircon Hf isotopic composition of two-mica granite and biotite granite

4.5.1. KLW-1

Eighteen zircon grains from sample KLW-1 were analyzed for Hf isotopic composition. The grain with a U–Pb age of 509 Ma (Table 2) yielded a $^{176}Hf/^{177}Hf$ value of 0.282301, with a calculated $\varepsilon_{Hf}(t)$ value of −5.85 and T_{DM} model age of 1839 Ma. The others yielded $^{176}Hf/^{177}Hf$ values of 0.282475 to 0.282617, and the calculated $\varepsilon_{Hf}(t)$ values range from −1.41 to +3.67, with T_{DM} model ages of 1193 to 1515 Ma (Table 3).

4.5.2. KLW-2

Seventeen zircon grains from sample KLW-2 were analyzed for Hf isotopic composition. Two grains with older U–Pb ages of 498 and 514 Ma (Table 2) yielded $^{176}Hf/^{177}Hf$ values of 0.282210 and 0.282190, with a calculated $\varepsilon_{Hf}(t)$ value of −9.46 and −9.83 and T_{DM} model age of 2055 and 2090 Ma, respectively. The others yielded $^{176}Hf/^{177}Hf$ values of 0.282528 to 0.282626, and the calculated $\varepsilon_{Hf}(t)$ values varied from +1.18 to +4.13, with T_{DM} model ages of 1172 to 1359 Ma (Table 3).

5. Discussion

5.1. Formation and evolution of the Kelumute No. 112 pegmatite

At present, it is widely accepted that pegmatite originates from the differentiation and evolution of a volatile-rich and peraluminous granitic residual melt with a long cooling history from liquid to solid in a relatively closed system (Zhang, 2001). The formation and evolution process of the magmatic, magmatic-hydrothermal transition and hydrothermal stages can be traced using studies of mineral association, U–Pb age and CL zircon features, as well as melt and fluid inclusions (unpublished data) in the Kelumute No. 112 pegmatite.

Zircons showing remnant oscillatory zoning and/or magmatic-origin rims, as well as melt inclusions found in zone I (albitization fine- to coarse-grained zone) and zone II (albitization blocky zone),

Table 1
U–Pb dating results of zircons from No.112 pegmatite, Kelumute, Altay (determined by LA-ICP-MS).

Spots	Th (ppm)	U (ppm)	Th/U	$^{207}Pb^*/^{206}Pb$	1σ	$^{207}Pb^*/^{235}U$	1σ	$^{206}Pb^*/^{238}U$	1σ	$^{207}Pb/^{235}U$	1σ	$^{206}Pb/^{238}U$	1σ
Zone I													
KLP-1.1	302	3907	0.08	0.13480	0.00390	0.71240	0.03169	0.03723	0.00071	546	19	236	4
KLP-1.2	723	2669	0.27	0.15884	0.00353	0.82454	0.01936	0.03762	0.00071	611	11	238	4
KLP-1.3	10838	8916	1.22	0.20469	0.00360	1.07782	0.02832	0.03772	0.00051	743	14	239	3
KLP-1.4	7752	7102	1.09	0.19248	0.00603	1.27696	0.04415	0.04786	0.00055	835	20	301	3
KLP-1.5	745	5092	0.15	0.21694	0.00563	1.16012	0.04287	0.03783	0.00050	782	20	239	3
KLP-1.6	580	7795	0.07	0.12447	0.00158	0.64266	0.01312	0.03703	0.00048	504	8	234	3
KLP-1.7	341	6668	0.05	0.16570	0.00542	0.90453	0.03564	0.03916	0.00041	654	19	248	3
KLP-1.8	7240	9882	0.73	0.21431	0.00223	1.09184	0.02140	0.03670	0.00049	749	10	232	3
KLP-1.11	1262	4191	0.30	0.26081	0.00221	1.34206	0.01495	0.03720	0.00031	864	6	235	2
KLP-1.12	358	9802	0.04	0.21816	0.00910	1.16594	0.06380	0.03746	0.00049	785	30	237	3
KLP-1.13	859	6043	0.14	0.13207	0.00367	0.68611	0.02453	0.03666	0.00041	530	15	232	3
KLP-1.14	1114	13777	0.08	0.15857	0.00437	0.85429	0.04968	0.03698	0.00100	627	27	234	6
KLP-1.15	1069	16834	0.06	0.15150	0.00143	0.78148	0.01200	0.03729	0.00049	586	7	236	3
KLP-1.17	6311	4662	1.35	0.30354	0.00660	1.68368	0.04881	0.04010	0.00089	1002	18	253	6
Zone II													
KLP-2.1	151	4635	0.03	0.05152	0.00162	0.24112	0.00543	0.03394	0.00075	219	4	215	5
KLP-2.2	56	4174	0.01	0.05115	0.00135	0.23984	0.00470	0.03400	0.00061	218	4	216	4
KLP-2.3	61	3270	0.02	0.05192	0.00221	0.21427	0.00712	0.02993	0.00079	197	6	190	5
KLP-2.4	17	1154	0.02	0.05295	0.00382	0.26724	0.01800	0.03661	0.00095	240	14	232	6
KLP-2.5	13	931	0.01	0.05203	0.00132	0.26758	0.00773	0.03722	0.00069	241	6	236	4
KLP-2.6	1279	10536	0.12	0.07465	0.01122	0.31938	0.04768	0.03103	0.00052	281	37	197	3
KLP-2.7	93	2667	0.03	0.05276	0.00265	0.26508	0.01256	0.03644	0.00061	239	10	231	4
KLP-2.8	234	3615	0.06	0.05994	0.00790	0.29832	0.03839	0.03610	0.00104	265	30	229	6
KLP-2.9	24	1719	0.01	0.05210	0.00094	0.26637	0.00564	0.03705	0.00054	240	5	235	3
KLP-2.10	133	3000	0.04	0.06495	0.00972	0.21986	0.03243	0.02455	0.00062	202	27	156	4
KLP-2.11	15	1253	0.01	0.05004	0.00213	0.19881	0.00775	0.02881	0.00049	184	7	183	3
KLP-2.12	16	1432	0.01	0.06822	0.00179	0.36297	0.01110	0.03836	0.00055	314	8	243	3
KLP-2.13	205	3829	0.05	0.09461	0.01819	0.20799	0.03940	0.01594	0.00052	192	33	102	3
KLP-2.14	253	3286	0.08	0.05603	0.00253	0.23135	0.00975	0.02994	0.00049	211	8	190	3
KLP-2.15	669	5119	0.13	0.15417	0.00931	0.51817	0.03018	0.02438	0.00039	424	20	155	2
KLP-2.16	713	17568	0.04	0.08392	0.01670	0.30626	0.06036	0.02647	0.00073	271	47	168	5
KLP-2.17	460	6420	0.07	0.05920	0.00573	0.21916	0.02070	0.02685	0.00057	201	17	171	4
KLP-2.18	30	801	0.04	0.05158	0.00237	0.20743	0.00777	0.02917	0.00078	191	7	185	5
KLP-2.19	92	2670	0.03	0.05479	0.00319	0.22223	0.01191	0.02942	0.00067	204	10	187	4
KLP-2.20	29	1322	0.02	0.05034	0.00259	0.21125	0.00966	0.03044	0.00072	195	8	193	5
KLP-2.21	38	1578	0.02	0.04685	0.00594	0.18165	0.02262	0.02812	0.00067	169	19	179	4
Zone III													
KLP-3.1	550	4526	0.12	0.09585	0.00654	0.66366	0.03987	0.05022	0.00163	517	24	316	10
KLP-3.2	1686	15620	0.11	0.05505	0.00185	0.18991	0.00498	0.02502	0.00053	177	4	159	3
KLP-3.3	1300	9865	0.13	0.06586	0.00506	0.26826	0.01992	0.02954	0.00059	241	16	188	4
KLP-3.4	797	2330	0.34	0.07932	0.00885	0.35758	0.03877	0.03270	0.00086	310	29	207	5
KLP-3.5	1188	4276	0.28	0.09153	0.00634	0.38467	0.02446	0.03048	0.00084	330	18	194	5
KLP-3.6	55	3996	0.01	0.05445	0.00273	0.22823	0.01043	0.03040	0.00062	209	9	193	4
KLP-3.7	2143	4422	0.48	0.08719	0.00853	0.36949	0.03121	0.03074	0.00152	319	23	195	9
KLP-3.8	615	1687	0.36	0.09979	0.00795	0.46132	0.03542	0.03353	0.00071	385	25	213	4
KLP-3.9	441	4330	0.10	0.05956	0.00332	0.28965	0.01470	0.03527	0.00081	258	12	223	5
KLP-3.10	724	3204	0.23	0.05482	0.00297	0.23980	0.01253	0.03172	0.00045	218	10	201	3
KLP-3.11	58	3062	0.02	0.04605	0.00654	0.18646	0.02533	0.02937	0.00122	174	22	187	8
KLP-3.12	101	13217	0.01	0.04997	0.00069	0.20719	0.01122	0.03026	0.00069	191	9	192	4
KLP-3.13	363	12722	0.03	0.05423	0.00077	0.20832	0.01463	0.03000	0.00199	192	12	191	12
KLP-3.14	1632	12664	0.13	0.09214	0.01812	0.38677	0.07298	0.03044	0.00169	332	53	193	11
KLP-3.15	1827	8741	0.21	0.05518	0.00128	0.22293	0.02509	0.02945	0.00089	204	21	187	6
KLP-3.16	1621	7352	0.22	0.05164	0.00097	0.20649	0.02257	0.02934	0.00085	191	19	186	5
KLP-3.17	605	3672	0.16	0.06936	0.00747	0.28295	0.02991	0.02959	0.00060	253	24	188	4
KLP-3.18	110	2211	0.05	0.05123	0.00066	0.20868	0.01433	0.02962	0.00022	192	12	188	1
KLP-3.19	613	4212	0.15	0.04605	0.01577	0.17149	0.05840	0.02701	0.00100	161	51	172	6
KLP-3.20	4294	23639	0.18	0.06069	0.00688	0.24468	0.02666	0.02924	0.00092	222	22	186	6
Zone V													
KLP-5.1	10	198	0.05	0.05162	0.00204	0.24251	0.00979	0.03439	0.00068	220	8	218	4
KLP-5.2	371	3534	0.11	0.05134	0.00060	0.24063	0.00380	0.03422	0.00061	219	3	217	4
KLP-5.3	5	274	0.02	0.05803	0.00177	0.26918	0.00843	0.03390	0.00062	242	7	215	4
KLP-5.4	114	2628	0.04	0.05347	0.00131	0.24698	0.00758	0.03395	0.00112	224	6	215	7
KLP-5.5	162	2531	0.06	0.05071	0.00079	0.24060	0.00505	0.03431	0.00058	219	4	217	4
KLP-5.6	33	761	0.04	0.05253	0.00147	0.25813	0.00830	0.03564	0.00074	233	7	226	5
KLP-5.7	129	1863	0.07	0.05044	0.00059	0.23875	0.00373	0.03432	0.00046	217	3	218	3
KLP-5.8	11	298	0.04	0.05045	0.00178	0.23967	0.00875	0.03449	0.00057	218	7	219	4
KLP-5.9	10	259	0.04	0.05675	0.00172	0.25209	0.00727	0.03273	0.00056	228	6	208	4
KLP-5.10	73	7085	0.01	0.05398	0.00123	0.25656	0.00791	0.03513	0.00106	232	6	223	7
KLP-5.11	27	413	0.07	0.05338	0.00171	0.25401	0.01009	0.03449	0.00075	230	8	219	5
KLP-5.12	8	121	0.07	0.05375	0.00256	0.25608	0.01263	0.03512	0.00075	231	10	223	5

(continued on next page)

Table 1 (*continued*)

Spots	Th (ppm)	U (ppm)	Th/U	$^{207}Pb^*/^{206}Pb$	1σ	$^{207}Pb^*/^{235}U$	1σ	$^{206}Pb^*/^{238}U$	1σ	$^{207}Pb/^{235}U$	1σ	$^{206}Pb/^{238}U$	1σ
Zone V													
KLP-5.13	342	2410	0.14	0.05486	0.00150	0.26599	0.01252	0.03513	0.00127	239	10	223	8
KLP-5.14	123	2573	0.05	0.05281	0.00085	0.23815	0.00423	0.03256	0.00034	217	3	207	2
KLP-5.15	234	4901	0.05	0.06057	0.00073	0.18211	0.00373	0.02207	0.00052	170	3	141	3
KLP-5.16	20	316	0.06	0.05053	0.00264	0.24217	0.01265	0.03511	0.00074	220	10	222	5
KLP-5.17	9	226	0.04	0.07443	0.00427	0.23432	0.01404	0.02293	0.00052	214	12	146	3
KLP-5.18	15	111	0.14	0.05103	0.00399	0.23656	0.01660	0.03425	0.00058	216	14	217	4
KLP-5.19	222	3548	0.06	0.05087	0.00043	0.24354	0.00312	0.03459	0.00035	221	3	219	2
KLP-5.20	16	298	0.05	0.05079	0.00202	0.24128	0.00974	0.03462	0.00048	219	8	219	3
Zone VI													
KLP-6.1	60	2954	0.02	0.05770	0.00585	0.25777	0.02542	0.03240	0.00076	233	21	206	5
KLP-6.2	37	4221	0.01	0.05014	0.00096	0.23169	0.00545	0.03357	0.00053	212	4	213	3
KLP-6.3	109	10484	0.01	0.05072	0.00354	0.22759	0.01543	0.03254	0.00055	208	13	206	3
KLP-6.4	255	5498	0.05	0.06088	0.00683	0.16791	0.01844	0.02000	0.00046	158	16	128	3
KLP-6.5	2641	27182	0.10	0.05699	0.00171	0.33281	0.00837	0.04236	0.00070	292	6	267	4
KLP-6.6	1042	5750	0.18	0.08538	0.00930	0.41119	0.04363	0.03493	0.00086	350	31	221	5
KLP-6.7	1604	6110	0.26	0.08162	0.00659	0.37381	0.02859	0.03322	0.00086	322	21	211	5
KLP-6.9	1207	22647	0.05	0.05627	0.00225	0.25562	0.00964	0.03294	0.00044	231	8	209	3
KLP-6.10	37	2206	0.02	0.06358	0.00276	0.26543	0.01105	0.03028	0.00038	239	9	192	2
KLP-6.11	49	6780	0.01	0.05302	0.00184	0.24919	0.00769	0.03409	0.00054	226	6	216	3
KLP-6.12	284	8182	0.03	0.05039	0.00801	0.21903	0.03470	0.03153	0.00043	201	29	200	3
KLP-6.13	41	5566	0.01	0.05393	0.00155	0.24971	0.00614	0.03358	0.00050	226	5	213	3
KLP-6.14	70	6495	0.01	0.06105	0.00570	0.27574	0.02550	0.03276	0.00042	247	20	208	3
KLP-6.15	66	9412	0.01	0.05726	0.00236	0.26656	0.01056	0.03376	0.00039	240	8	214	2
KLP-6.16	72	6402	0.01	0.05558	0.00345	0.25521	0.01555	0.03330	0.00039	231	13	211	2
KLP-6.17	16	3950	0.004	0.05289	0.00210	0.25124	0.00790	0.03445	0.00083	228	6	218	5
KLP-6.18	45	5933	0.01	0.05255	0.00156	0.23702	0.00674	0.03271	0.00028	216	6	208	2
KLP-6.19	213	7180	0.03	0.05661	0.00364	0.25523	0.01607	0.03270	0.00042	231	13	207	3
KLP-6.20	360	6468	0.06	0.06000	0.00497	0.28920	0.02371	0.03496	0.00041	258	19	222	3

Table 2
U–Pb dating results of zircon from granites, intruded by No.112 pegmatite, Kelumute, Altay (determined by LA-ICP-MS).

Spots	Th (ppm)	U (ppm)	Th/U	$^{207}Pb^*/^{206}Pb$	1σ	$^{207}Pb^*/^{235}U$	1σ	$^{206}Pb^*/^{238}U$	1σ	$^{207}Pb/^{235}U$	1σ	$^{206}Pb/^{238}U$	1σ
Two mica granite													
KLW-1.1	133	283	0.47	0.06144	0.00264	0.68243	0.02499	0.08219	0.00184	528	15	509	11
KLW-1.2	338	800	0.42	0.06988	0.00312	0.64223	0.03929	0.06644	0.00267	504	24	415	16
KLW-1.3	208	332	0.63	0.06008	0.00271	0.58731	0.02566	0.07116	0.00149	469	16	443	9
KLW-1.4	99	303	0.33	0.07202	0.00367	0.67748	0.02442	0.07017	0.00151	525	15	437	9
KLW-1.5	380	1022	0.37	0.05792	0.00099	0.56314	0.01243	0.07083	0.00138	454	8	441	8
KLW-1.6	187	365	0.51	0.05634	0.00151	0.56018	0.01690	0.07308	0.00150	452	11	455	9
KLW-1.7	41	121	0.34	0.05743	0.00411	0.57989	0.03813	0.07498	0.00192	464	25	466	12
KLW-1.8	82	218	0.38	0.05784	0.00222	0.56944	0.02253	0.07294	0.00104	458	15	454	6
KLW-1.9	258	682	0.38	0.05951	0.00136	0.59120	0.01640	0.07212	0.00127	472	10	449	8
KLW-1.10	75	252	0.30	0.05627	0.00202	0.54735	0.01989	0.07098	0.00123	443	13	442	7
KLW-1.11	151	525	0.29	0.05672	0.00141	0.56558	0.01653	0.07184	0.00088	455	11	447	5
KLW-1.12	114	247	0.46	0.05557	0.00149	0.53504	0.01694	0.06919	0.00087	435	11	431	5
KLW-1.13	111	682	0.16	0.05599	0.00274	0.54126	0.02647	0.06990	0.00072	439	17	436	4
KLW-1.14	34	146	0.23	0.05604	0.00232	0.57227	0.02400	0.07372	0.00087	459	15	459	5
KLW-1.15	99	383	0.26	0.05716	0.00153	0.57732	0.01579	0.07289	0.00071	463	10	454	4
KLW-1.16	173	460	0.38	0.05688	0.00147	0.56034	0.01594	0.07075	0.00077	452	10	441	5
KLW-1.17	194	293	0.66	0.05677	0.00205	0.56883	0.02073	0.07219	0.00079	457	13	449	5
KLW-1.18	85	367	0.23	0.05430	0.00135	0.54215	0.01432	0.07164	0.00058	440	9	446	3
Biotite granite													
KLW-2.1	95	549	0.17	0.05753	0.00121	0.55587	0.01331	0.07063	0.00158	449	9	440	10
KLW-2.2	39	357	0.11	0.05754	0.00147	0.57188	0.01621	0.07234	0.00128	459	10	450	8
KLW-2.3	158	353	0.45	0.05711	0.00171	0.65906	0.02412	0.08300	0.00132	514	15	514	8
KLW-2.4	40	458	0.09	0.05657	0.00139	0.57555	0.01512	0.07478	0.00168	462	10	465	10
KLW-2.5	52	338	0.15	0.05732	0.00151	0.58839	0.01541	0.07496	0.00123	470	10	466	7
KLW-2.6	134	255	0.52	0.05671	0.00158	0.57008	0.01708	0.07346	0.00128	458	11	457	8
KLW-2.7	306	416	0.74	0.06002	0.00266	0.58183	0.02270	0.07125	0.00111	466	15	444	7
KLW-2.8	320	519	0.62	0.06334	0.00410	0.64519	0.04471	0.07355	0.00112	506	28	458	7
KLW-2.9	41	372	0.11	0.05693	0.00216	0.58053	0.02511	0.07397	0.00175	465	16	460	11
KLW-2.10	264	456	0.58	0.05697	0.00138	0.58709	0.01631	0.07481	0.00160	469	10	465	10
KLW-2.11	242	313	0.78	0.05702	0.00246	0.63365	0.02802	0.08029	0.00136	498	17	498	8
KLW-2.12	357	474	0.75	0.05993	0.00164	0.61131	0.02044	0.07355	0.00127	484	13	457	8
KLW-2.13	62	235	0.26	0.05621	0.00203	0.58645	0.02174	0.07550	0.00098	469	14	469	6
KLW-2.14	131	637	0.21	0.05607	0.00111	0.55879	0.01334	0.07183	0.00077	451	9	447	5
KLW-2.15	59	407	0.14	0.05645	0.00128	0.57293	0.01567	0.07327	0.00100	460	10	456	6

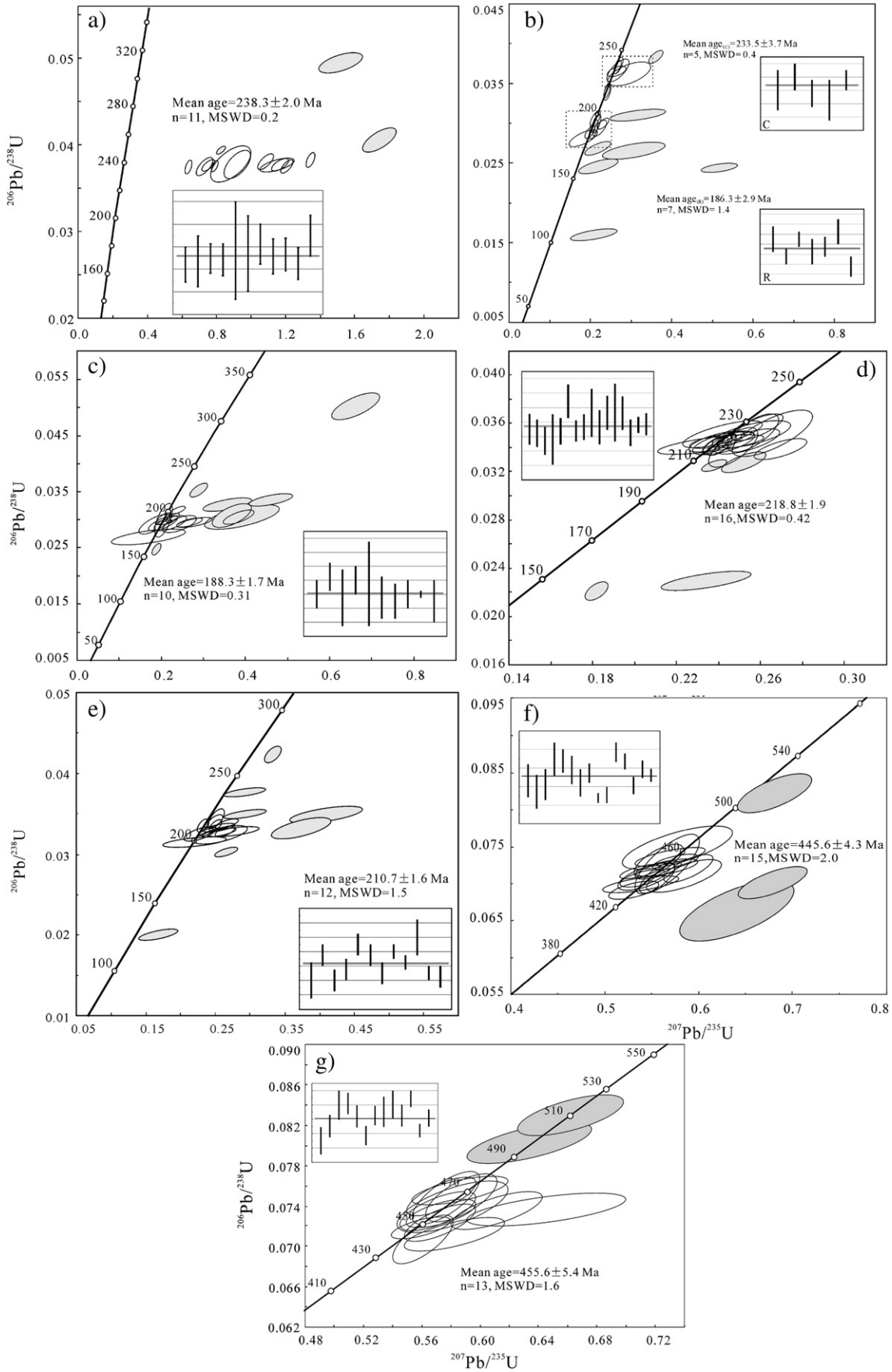

Fig. 5. Concordia and weighted average diagrams showing the LA-ICP-MS U – Pb ages of zircon grains from samples KLP-1(a), KLP-2(b), KLP-3(c), KLP-5(d), KLP-6 (e), KLW-1(f) and KLW-2(g). Mean ages were calculated from age spot without padding gray, error ovals are 1 sigma and mean ages given as 2 sigma.C—crystallization, R—recrystallization.

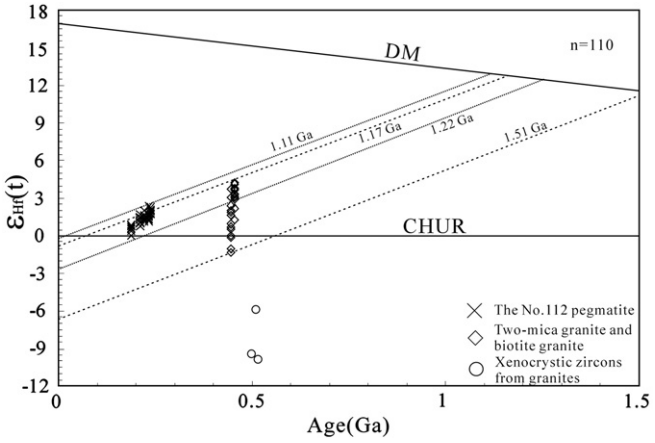

Fig. 6. Diagram of $\varepsilon_{Hf}(t)$ values versus crystallizing ages for zircons from the Kelumute No.112 pegmatite and wall rocks of granites in the Chinese Altay.

indicated that these two textual zones were formed in a magmatic stage. Moreover, zircons from both these textural zones have older ages than the other textural zones (238.3 ± 2.0 Ma, 233.5 ± 3.7 Ma, respectively; Fig. 5a, b), indicating that they were formed soon after cooling of the No. 112 pegmatite magma. Most zircons from these two zones showing blurred and/or weak oscillatory zoning in their mantles and/or rims and no zoning in their cores, rather than a speckled, taxitic or spongy structure (Fig. 4a, b), and were characterized by high U and/or Th content and insignificant ages with low concordance rates due to radioactive Pb loss. All of these characteristics suggest that the early textural zones underwent metamictization, late fluid alteration and recrystallization (Wu and Zheng, 2004).

Abundant fluid-melt inclusions were found in spodumenes from zone III, indicating that zone III was formed during a magmatic–hydrothermal stage. Zircons from this zone, characterized by black and homogenous composition without oscillatory zoning, are similar to hydrothermal zircons, such as those reported from the Boggy Plain zoned pluton in Eastern Australia (Hoskin, 2005), mylonitized granite from the Tianger mountain area, Central Tianshan (Zhu and Song, 2006), Xianshuiquan gneissic granite, East Tianshan in Xinjiang, China (Tang et al., 2008) and the gold-bearing quartz vein of Rushan in East Jiaozhou, China (Hu et al., 2004). Ten spots from the primary or low-metamictization zircon domains yielded a weighted mean $^{206}Pb/^{238}U$ age of 188.3 ± 1.7 Ma, equal to the recrystallization age of 186.3 ± 2.9 Ma from zircons of zone II within error limits, representing the age of fluid activity during hydrothermal stage.

CL images of zircons from zone V show a striking contrast between bright and dark domains. The dark domains show weak CL and homogenous, higher U and Th content with or without oscillatory zoning of the primary zircon domains. The bright domains are characterized by intense CL, a homogenous or spongy, mottled texture, and lower Th and U content and represent the recrystallization domains of the zircons. As the weighted mean $^{206}Pb/^{238}U$ ages for both domains are highly consistent and within the limit of error, we suggest that the crystallization and recrystallization of zircons happened almost simultaneously, indicating coexisting magma and hydrothermal systems, namely, the magmatic–hydrothermal transition stage. There is other evidence for fluid–melt inclusions in quartz from zone V to support this hypothesis.

The occurrence of quartz core signifies the ending of the magmatic–hydrothermal stage and the beginning of the hydrothermal stage and is characterized by abundant fluid inclusions (Wu and Zhu, 1995; Wu et al., 1994; unpublished data of authors). Metasomatic relict texture and harbor texture in primary zircons are due to intense hydrothermal alteration of the quartz core of the Kelumute No. 112 pegmatite (Fig. 4e). Thus, the weighted mean $^{206}Pb/^{238}U$ age of 210.7 ± 1.6 Ma represents the upper limit of the starting time of the hydrothermal stage.

In conclusion, the Kelumute No. 112 pegmatite magma intruded into the Paleozoic Jideke two-mica granite at approximately 238.3 ± 2.0 Ma, and then began its fractional crystallization. Because of the large temperature difference between the magma and the wall rock, the rapidly cooling crystallization was characterized by development of fine-grained crystal, namely albitization of a fine- to coarse-grained zone (I) and albitization blocky zone (II). After their formation and the untimely end of the magma stage, the pegmatite magma crossed into a magmatic–hydrothermal transition stage characterized by coexistence of crystal, melt and fluid phases. As a result, the quartz–albite–spodumene zone (III), albite–quartz–muscovite zone (IV) and saccharoidal albite zone (V) were formed. Finally, pegmatite magma evolved to the hydrothermal stage, characterized by the appearance of a quartz core (VI).

The formation and evolution of the Kelumute No. 112 pegmatite is significantly different from that of the world-famous Koktokay No. 3 pegmatite. One difference is that a potassium evolution stage characterized by a graphic microcline zone and a blocky microcline zone in the No. 3 pegmatite was absent during the evolution of the No. 112 pegmatite. Another difference is that the No. 112 pegmatite magma evolved more quickly from the magmatic to magmatic–hydrothermal transition stage than did the Koktokay No. 3 pegmatite. The magmatic stage in the No. 112 pegmatite consisted only of zone I and II in a proportion of 25%, but in the No. 3 pegmatite, the magmatic stage included zone I to IV, with a higher proportion of 70% (Zhang, 2001; Zhu et al., 2000). The differences may be explained by two possible causes: (1) the main alkali metal in the initial magma of the Kelumute No. 112 pegmatite was sodium, with little potassium; or (2) the initial magma of the No. 112 pegmatite underwent a high degree of fractional crystallization in the magma chamber before cooling, and the graphic microcline zone and blocky microcline zone were retained in the magma chamber.

5.2. Time scale of magmatic–hydrothermal evolution

Accurate dating of magmatic, magmatic–hydrothermal transition and hydrothermal stages during the evolution of pegmatite is a continuing research focus due to limited available data. The nature and evolution of the magmatic–hydrothermal transition stage, which is identified qualitatively as a transition stage between the magmatic and hydrothermal stage characterized by coexisting of melt, crystal and fluid phases (Burnham and Ohmoto, 1980; London, 1986), are still not clear. The traditional view suggests that the formation of pegmatite underwent a high degree of fractional crystallization with a long cooling history. Some scholars have recently proposed that the cooling rate of pegmatite magma is much faster than in this traditional conception (London, 2005; Morgan and London, 1999). Therefore, accurate dating of magmatic, magmatic–hydrothermal transition and hydrothermal stages is key to understanding the cooling history of the Kelumute No. 112 pegmatite and other pegmatites around the world.

As for the world famous Koktokay No. 3 pegmatite, characterized by the concentric ring structure of nine textural zones, it was initially thought to be the product of fractional crystallization with a long history over ~100 Ma (Zou et al., 1986). Chen et al. (1999) proposed that the fractional crystallization process lasted ~30 Ma, based on their determination of Ar–Ar ages from K-rich minerals. However, these studies failed to distinguish the duration of the magmatic–hydrothermal transition stage from the evolution of magma. By investigating this duration, Zhu et al. (2000) speculated that the period began from the formation of the cleavelandite–spodumene zone (5th) to the textural zone before the occurrence of the quartz core zone (9th), or pollucite, which represents the subsolid condition. Recently, according to zircon SHRIMP U–Pb ages from zones I, V and VII of the Koktokay No. 3 pegmatite, Wang et al. (2007) suggested

Table 3
Hf isotopic compositions of the No.112 pegmatite and wall rocks of granites (determined by LA-MC-ICP-MS).

Sample spot	$^{176}Yb/^{177}Hf$	$^{176}Lu/^{177}Hf$	1σ	$^{176}Hf/^{177}Hf$	1σ	Age (Ma)	$\varepsilon_{Hf}(t)$	1 σ	T^{C}_{DM} (Ma)	1 σ	$f_{Lu/Hf}$
KLP-1											
1	0.001314	0.000017	0.000001	0.282682	0.000008	238	2.06	0.28	1135	19	−0.999
2	0.001430	0.000021	0.000001	0.282681	0.000009	238	2.02	0.32	1137	21	−0.999
3	0.003419	0.000048	0.000003	0.282681	0.000007	238	2.01	0.25	1138	16	−0.999
4	0.001306	0.000018	0.000001	0.282682	0.000007	238	2.06	0.25	1135	16	−0.999
5	0.006356	0.000087	0.000003	0.282682	0.00001	238	2.04	0.35	1136	23	−0.997
6	0.011519	0.000168	0.000007	0.282682	0.000011	238	2.03	0.39	1136	26	−0.995
7	0.001731	0.000025	0.000001	0.282672	0.000006	238	1.70	0.21	1157	14	−0.999
8	0.007525	0.000098	0.000004	0.282684	0.000006	238	2.11	0.21	1131	14	−0.997
9	0.003863	0.000051	0.000002	0.282688	0.000011	238	2.26	0.39	1122	26	−0.998
10	0.003240	0.000068	0.000001	0.282681	0.000008	238	2.01	0.28	1138	19	−0.998
11	0.007584	0.000111	0.000003	0.282675	0.00001	238	1.79	0.35	1152	23	−0.997
12	0.002664	0.000038	0.000003	0.282680	0.000009	238	1.98	0.32	1140	21	−0.999
13	0.002150	0.000033	0.000001	0.282683	0.000008	238	2.09	0.28	1133	19	−0.999
14	0.003128	0.000045	0.000002	0.282680	0.000009	238	1.98	0.32	1140	21	−0.999
15	0.002455	0.000039	0.000001	0.282673	0.000009	238	1.73	0.32	1155	21	−0.999
KLP-2											
1	0.000101	0.0000011	0.0000001	0.282673	0.000008	233	1.62	0.28	1158	19	−1.000
2	0.000394	0.0000059	0.0000006	0.282663	0.000009	233	1.26	0.32	1181	21	−1.000
3	0.004431	0.0000522	0.0000011	0.282674	0.000016	233	1.65	0.57	1157	37	−0.998
4	0.003265	0.0000422	0.0000009	0.282674	0.000014	233	1.65	0.50	1157	33	−0.999
5	0.000529	0.0000074	0.0000003	0.282675	0.000006	233	1.69	0.21	1154	14	−1.000
6	0.00339	0.0000433	0.0000014	0.282694	0.000011	233	2.35	0.39	1112	26	−0.999
7	0.000691	0.0000105	0.0000005	0.282675	0.000009	233	1.69	0.32	1154	21	−1.000
8	0.000736	0.0000082	0.0000001	0.282672	0.000007	233	1.58	0.25	1161	16	−1.000
9	0.000129	0.0000016	0.0000002	0.282674	0.000005	233	1.65	0.18	1156	12	−1.000
10	0.000263	0.0000033	0.0000003	0.282675	0.000006	233	1.69	0.21	1154	14	−1.000
11	0.000098	0.000001	0.0000001	0.282665	0.000007	233	1.34	0.25	1176	16	−1.000
12	0.000285	0.000004	0.0000003	0.282672	0.000006	233	1.58	0.21	1161	14	−1.000
13	0.001924	0.0000223	0.0000008	0.282673	0.000011	233	1.61	0.39	1159	26	−0.999
14	0.000488	0.0000071	0.0000007	0.282660	0.000009	233	1.16	0.32	1188	21	−1.000
15	0.004001	0.0000472	0.0000019	0.282670	0.000011	233	1.50	0.39	1166	26	−0.999
KLP-3											
1	0.000132	0.00000203	0.00000009	0.282670	0.000005	188	0.53	0.18	1193	12	−1.000
2	0.000798	0.00001382	0.00000055	0.282672	0.000008	188	0.60	0.28	1189	19	−1.000
3	0.000339	0.00000465	0.0000001	0.282673	0.000009	188	0.64	0.32	1187	21	−1.000
4	0.000086	0.00000153	0.00000004	0.282670	0.000009	188	0.53	0.32	1193	21	−1.000
5	0.000161	0.00000244	0.00000005	0.282671	0.000009	188	0.57	0.32	1191	21	−1.000
6	0.000138	0.0000021	0.00000009	0.282676	0.000009	188	0.74	0.32	1180	21	−1.000
7	0.000235	0.00000348	0.00000023	0.282670	0.000015	188	0.53	0.53	1193	35	−1.000
8	0.000054	0.00000089	0.00000005	0.282656	0.000012	188	0.03	0.42	1225	28	−1.000
9	0.000116	0.00000222	0.0000001	0.282666	0.000016	188	0.39	0.57	1202	37	−1.000
10	0.000177	0.00000259	0.00000012	0.282673	0.000017	188	0.64	0.60	1187	40	−1.000
11	0.000127	0.0000019	0.00000007	0.282680	0.000014	188	0.88	0.50	1171	33	−1.000
12	0.000161	0.00000297	0.00000016	0.282676	0.000014	188	0.74	0.50	1180	33	−1.000
13	0.000087	0.00000163	0.00000004	0.282672	0.000013	188	0.60	0.46	1189	30	−1.000
14	0.000372	0.00000504	0.00000034	0.282667	0.000014	188	0.42	0.50	1200	33	−1.000
15	0.000684	0.00001338	0.00000095	0.282672	0.000014	188	0.60	0.50	1189	33	−1.000
KLP-5											
1	0.000030	0.00000043	0.00000002	0.282673	0.000006	219	1.31	0.21	1167	14	−1.000
2	0.000020	0.00000041	0.00000002	0.282672	0.000009	219	1.27	0.32	1169	21	−1.000
3	0.000115	0.00000173	0.00000006	0.282675	0.00001	219	1.38	0.35	1163	23	−1.000
4	0.000031	0.00000026	0.00000002	0.282669	0.000007	219	1.17	0.25	1176	16	−1.000
5	0.000049	0.00000053	0.00000003	0.282679	0.000005	219	1.52	0.18	1154	12	−1.000
6	0.000125	0.00000166	0.00000006	0.282676	0.000006	219	1.42	0.21	1161	14	−1.000
7	0.000024	0.0000002	0.00000003	0.282674	0.000007	219	1.35	0.25	1165	16	−1.000
8	0.000203	0.00000265	0.00000006	0.282683	0.00001	219	1.66	0.35	1145	23	−1.000
9	0.000059	0.00000087	0.00000004	0.282673	0.000006	219	1.31	0.21	1167	14	−1.000
10	0.000027	0.00000036	0.00000004	0.282683	0.000008	219	1.66	0.28	1145	19	−1.000
11	0.000025	0.00000024	0.00000004	0.282673	0.00001	219	1.31	0.35	1167	23	−1.000
12	0.000017	0.00000035	0.00000003	0.282672	0.000012	219	1.27	0.42	1169	28	−1.000
13	0.000031	0.00000062	0.00000004	0.282673	0.000013	219	1.31	0.46	1167	30	−1.000
14	0.000026	0.00000035	0.00000003	0.282693	0.000008	219	2.02	0.28	1122	19	−1.000
15	0.000016	0.00000027	0.00000002	0.282676	0.000007	219	1.42	0.25	1161	16	−1.000
KLP-6											
1	0.006083	0.000054	0.000001	0.282682	0.000008	211	1.56	0.28	1149	19	−0.998
2	0.007548	0.000085	0.000011	0.282680	0.000008	211	1.49	0.28	1154	19	−0.997
3	0.002732	0.000039	0.000001	0.282681	0.000007	211	1.53	0.25	1151	16	−0.999
4	0.009267	0.000103	0.000004	0.282676	0.000008	211	1.34	0.28	1163	19	−0.997
5	0.010765	0.000102	0.000002	0.282664	0.000008	211	0.92	0.28	1190	19	−0.997

(continued on next page)

Table 3 (*continued*)

Sample spot	$^{176}Yb/^{177}Hf$	$^{176}Lu/^{177}Hf$	1σ	$^{176}Hf/^{177}Hf$	1σ	Age (Ma)	$\varepsilon_{Hf}(t)$	1 σ	T^{C}_{DM} (Ma)	1 σ	$f_{Lu/Hf}$
KLP-6											
6	0.023134	0.000242	0.000022	0.282690	0.000009	211	1.82	0.32	1133	21	−0.993
7	0.008029	0.000076	0.000004	0.282664	0.000008	211	0.92	0.28	1190	19	−0.998
8	0.028482	0.000295	0.000023	0.282673	0.000014	211	1.21	0.50	1172	33	−0.991
9	0.008407	0.000091	0.000003	0.282681	0.000007	211	1.52	0.25	1152	16	−0.997
10	0.006004	0.000061	0.000003	0.282682	0.000008	211	1.56	0.28	1149	19	−0.998
11	0.013231	0.000159	0.000012	0.282682	0.000009	211	1.55	0.32	1150	21	−0.995
12	0.002107	0.000027	0.000002	0.282680	0.000007	211	1.50	0.25	1153	16	−0.999
13	0.006490	0.000067	0.000003	0.282669	0.000008	211	1.10	0.28	1178	19	−0.998
14	0.005728	0.000054	0.000002	0.282671	0.000008	211	1.17	0.28	1174	19	−0.998
15	0.004620	0.000041	0.000001	0.282681	0.000008	211	1.53	0.28	1151	19	−0.999
KLW-1											
1	0.121343	0.002223	0.000068	0.282617	0.000014	446	3.67	0.50	1191	33	−0.933
2	0.110542	0.001995	0.000024	0.282578	0.00001	446	2.36	0.35	1274	23	−0.940
3	0.210584	0.003715	0.00016	0.282539	0.000014	446	0.47	0.50	1393	33	−0.888
4	0.112996	0.002081	0.000042	0.282567	0.000012	446	1.95	0.42	1300	28	−0.937
5	0.065250	0.001146	0.000057	0.282475	0.000018	446	−1.03	0.64	1488	42	−0.965
6	0.143598	0.002577	0.000071	0.282561	0.000012	446	1.59	0.43	1323	28	−0.922
7	0.069241	0.001298	0.000041	0.282520	0.000028	446	0.51	0.99	1391	66	−0.961
8	0.102345	0.002088	0.000047	0.282563	0.000015	446	1.80	0.53	1309	35	−0.937
9	0.140871	0.002674	0.000042	0.282511	0.000018	446	−0.21	0.64	1436	42	−0.919
10	0.130696	0.002416	0.000072	0.282475	0.000017	446	−1.41	0.60	1512	40	−0.927
11	0.106135	0.001964	0.000031	0.282530	0.000015	446	0.67	0.53	1381	35	−0.941
12	0.124286	0.002265	0.000056	0.282511	0.000013	446	−0.09	0.46	1429	31	−0.932
13	0.113059	0.0022	0.000021	0.282557	0.000013	446	1.56	0.46	1325	31	−0.934
14	0.145408	0.002653	0.00007	0.282542	0.000018	446	0.89	0.64	1367	42	−0.920
15	0.104613	0.002111	0.000096	0.282596	0.00002	446	2.96	0.71	1236	47	−0.936
16	0.092970	0.001893	0.000029	0.282565	0.000011	446	1.93	0.39	1301	26	−0.943
17	0.062850	0.001191	0.000047	0.282301	0.000016	509	−5.85	0.57	1875	38	−0.964
18	0.135561	0.0026	0.00016	0.282530	0.000016	446	0.48	0.57	1393	38	−0.922
KLW-2											
1	0.133090	0.002444	0.000018	0.282610	0.000013	456	3.57	0.46	1206	30	−0.926
2	0.138873	0.002459	0.000038	0.282626	0.000013	456	4.13	0.46	1170	30	−0.926
3	0.115941	0.002122	0.000033	0.282597	0.000015	456	3.20	0.53	1229	35	−0.936
4	0.181008	0.003471	0.0001	0.282601	0.000011	456	2.94	0.39	1246	26	−0.895
5	0.084749	0.001479	0.00016	0.282561	0.000011	456	2.12	0.39	1297	26	−0.955
6	0.127727	0.002425	0.000089	0.282623	0.000013	456	4.03	0.46	1176	30	−0.927
7	0.100641	0.001902	0.000045	0.282588	0.000017	456	2.95	0.60	1245	40	−0.943
8	0.104114	0.00199	0.000041	0.282588	0.000019	456	2.92	0.67	1246	45	−0.940
9	0.139326	0.002655	0.000037	0.282596	0.000013	456	3.01	0.46	1241	30	−0.920
10	0.084562	0.001628	0.000016	0.282190	0.000035	514	−9.83	1.24	2122	83	−0.951
11	0.084564	0.001628	0.000016	0.282210	0.000036	498	−9.46	1.27	2078	86	−0.951
12	0.115963	0.002262	0.000068	0.282591	0.000018	456	2.95	0.64	1245	42	−0.932
13	0.041400	0.000724	0.00014	0.282528	0.000015	456	1.18	0.53	1356	35	−0.978
14	0.039771	0.000805	0.000078	0.282599	0.000015	456	3.67	0.53	1199	35	−0.976
15	0.141192	0.002822	0.000025	0.282591	0.000013	456	2.78	0.46	1255	30	−0.915
16	0.103955	0.002003	0.000096	0.282598	0.00001	456	3.27	0.36	1224	23	−0.940
17	0.099427	0.001942	0.00011	0.282610	0.000013	456	3.72	0.46	1196	31	−0.942

$\varepsilon_{Hf}(t) = 10{,}000 \times \{[(^{176}Hf/^{177}Hf)_S - (^{176}Lu/^{177}Hf)_S \times (e^{\lambda t} - 1)]/[(^{176}Hf/^{177}Hf)_{CHUR,0} - (^{176}Lu/^{177}Hf)_{CHUR} \times (e^{\lambda t} - 1)] - 1\}$.
$T_{DM} = 1/\lambda \times \ln\{1 + [(^{176}Hf/^{177}Hf)_S - (^{176}Hf/^{177}Hf)_{DM}]/[(^{176}Lu/^{177}Hf)_S - (^{176}Lu/^{177}Hf)_{DM}]\}$.
$f_{Lu/Hf} = (^{176}Lu/^{177}Hf)_S/(^{176}Lu/^{177}Hf)_{CHUR} - 1$.
$T^{C}_{DM} = t + 1/\lambda \times \ln\{1 + [(^{176}Hf/^{177}Hf)_{S,t} - (^{176}Hf/^{177}Hf)_{DM,t}]/[(^{176}Lu/^{177}Hf)_{LC} - (^{176}Lu/^{177}Hf)_{DM}]\}$.
Where, $k = 1.867 \times 10^{-11}$ year^{-1} (Soderlund et al., 2004); $(^{176}Lu/^{177}Hf)_S$ and $(^{176}Hf/^{177}Hf)_S$ are the measured values of the samples; $(^{176}Lu/^{177}Hf)_{CHUR} = 0.0332$ and $(^{176}Hf/^{177}Hf)_{CHUR,0} = 0.282772$ (Blichert-Toft and Albarède, 1997); $(^{176}Lu/^{177}Hf)_{DM} = 0.0384$ and $(^{176}Hf/^{177}Hf)_{DM} = 0.28325$ (Griffin et al., 2002); $(^{176}Lu/^{177}Hf)_{LC} = 0.019$; t = crystallization time of zircon.

that the age of 220 ± 9 Ma for zone I probably represents the early stage of pegmatite formation, and the age of 198 ± 7 Ma obtained for zone V represents the final stage of the pegmatite formation, or alternatively, the time from the hydrothermal stage. Therefore, these authors posited that the dates from 220 ± 9 to 198 ± 7 Ma reflect a period of magmatic–hydrothermal activity and can be regarded as the formation age of the No. 3 pegmatite. The time span from 213 ± 6 Ma to 198 ± 7 Ma corresponds to the latest stage of hydrothermal alteration.

Abundant fluid–melt inclusions are enclosed in the spodumene of zone III of the Kelumute No. 112 pegmatite (Wu and Zhu, 1995; Wu et al., 1994; unpublished data of the authors), indicating that the fluid phase exsolved after the formation of albitization blocky zone (2th). In other words, the magmatic–hydrothermal stage of No. 112 pegmatite lasted from the quartz–albite–spodumene zone (3th) to the saccharoidal albite zone (5th) until the appearance of quartz core zone (6th), which represents the beginning of the hydrothermal stage.

It has been determined that fluid phase exsolution and spodumenes crystallization from pegmatite magma happened simultaneously in the Kelumute No. 112 pegmatite, consistent with the circumstances of the Koktokay No. 3 pegmatite, the Altay and the Tanco pegmatite of Canada (London, 1986; Lu et al., 1996). According to zircon U–Pb ages of five texture zones from the No. 112 pegmatite in this paper, we propose that 238.3 ± 2.0 Ma reflects the upper limit of the pegmatite formation, and 188.3 ± 1.7 Ma most likely represents the formation time of the hydrothermal zircons during the final stage. Therefore, the time span

from 238.3 ± 2.0 to 233.5 ± 3.7 Ma (temporal scale of ~5 Ma) may reflect evolutionary time in the magmatic stage; the span from 210.7 ± 1.6 Ma to 188.3 ± 1.7 Ma (temporal scale of ~22 Ma) most likely represents the timing and duration of the hydrothermal stage; and the span from 233.5 ± 3.7 Ma to 210.7 ± 1.6 Ma (temporal scale of ~23 Ma) represents the maximum duration of the magmatic–hydrothermal transition stage of the Kelumute No. 112 pegmatite.

5.3. Source nature of the Kelumute No. 112 pegmatite magma

Granitic pegmatite is generally considered a product of volatile-rich residual magma via differentiation of parental granitic magma. Even when no granite is exposed on the surface, pegmatite is assumed to have genetic relationship with deeply buried granite (Fuertes-Fuente et al., 2000; Jolliff et al., 1992; London et al., 1990; Webster et al., 1997).

The relationship between the Kelumute No. 112 pegmatite and the host rocks of the Jideke two-mica granite is still unknown. Zircon U–Pb ages of 445.6 ± 4.3 and 455.6 ± 5.4 Ma for the Jideke two-mica granite and biotite granite indicate that they were formed in the Middle Paleozoic as synorogenic granites (460 to 380 Ma). However, the zircon U–Pb age of 238.3 ± 2.0 Ma for zone I from the Kelumute No. 112 pegmatite suggests that its formation is related to Mesozoic magma activity, which has previously been identified with the production of anorogenic magmatism (Wang et al., 2007; Zhang et al., 1994). As there is a significant temporal difference between pegmatite and granite, it is too difficult to establish a direct genetic relationship. Thus, it is reasonable to speculate that there is no genetic relationship between the Kelumute No. 112 pegmatite and the wall rocks of the two-mica granite and biotite granite.

This result differs from that obtained from the zircon Hf isotope of the Middle and Late Paleozoic granites in the south domain (unit 4 and 5 in Fig. 1) of the Chinese Altay (Cai et al., 2011a; Tong, 2006). Zircons from the Jideke two-mica granite (KLW-1) and biotite granite (KLW-2) yielded lower positive $\varepsilon_{Hf}(t)$ values, close to CHUR but obviously deviating from the DM line (Fig. 6) and suggesting that magmas originated from two-end mixtures (crust and mantle components), with a larger proportion of old crustal components in the magma source. These two Paleozoic granites with lower zircon $\varepsilon_{Hf}(t)$ values (−1.41 to +4.13) have magma sources derived from mixing of minor mantle-derived material with ancient crustal components (Fig. 6). Furthermore, these two Paleozoic granites with Proterozoic T_{DM} model age and minor xenocrystic zircons from the two granites with larger negative $\varepsilon_{Hf}(t)$ (−5.85 to −9.83) indicate that ancient crustal materials likely derived from Precambrian basements, or metasediments of the Habahe Group. Recently, more studies have provided evidence for the existence of an Altay microcontinent (Hu et al., 2000; Li et al., 2006; Tong, 2006; Wang et al., 2009; Windley et al., 2002; Wang et al., 2003a). The Habahe Group, which has been previously identified with the Precambrian microcontinent, mainly derived from the Cambrian–Early Ordovician continental arc (Long et al., 2007), analogous to greywackes from the continental arc or an active continental margin (Long et al., 2008, 2010). Although Cai et al. (2011b) suggested the Habahe Group as the source rocks for these Paleozoic granites, we support a model that involves mixing of the Precambrian basement (Proterozoic crust) with mantle-derived materials, as Habahe Group metasediments are too young to play a role in the formation of these Middle Paleozoic granites. It was previously demonstrated that Early–Middle Paleozoic granites (500 to 370 Ma) from the central Chinese Altay show lower positive $\varepsilon_{Hf}(t)$ and $\varepsilon_{Nd}(t)$ and older T_{DM} model ages than those from the southern Chinese Altay, indicating that Precambrian components most likely exist in the central Chinese Altay (Tong et al., 2006a,b; Wang et al., 2009). If true, this most likely implies that Precambrian basements in the Chinese Altay represent an immature crust whose mantle-derived component was involved in differentiation between the crust and mantle in Precambrian era. Recently, according to zircon SHRIMP U–Pb ages of granites and basalts, Li et al. (2006) suggested that the Chinese Altay most likely experienced four major events during the Proterozoic era and that the Altay–Mongolia microcontinent is an immature continent mainly composed of Proterozoic materials. Long et al. (2007) and Sun et al. (2008) proposed that a significant amount of Neoproterozoic zircons from the Chinese Altay were derived from Neoproterozoic magmatic arcs near the south margin of the Siberia Craton, with older zircons from a more distal source in the craton. Combined with granitoids from the Junggar block, Wang et al. (2004a) suggested that granitoids with positive $\varepsilon_{Nd}(t)$ values from the mountains of Altay, central Tianshan, Kunlun and Junggar terranes indicate an immature crust-derived source.

The Zircon Hf isotope of the Kelumute No. 112 pegmatite showed relatively lower positive $\varepsilon_{Hf}(t)$ values (+0.03 to +2.35), with T_{DM} model ages of 1112–1225 Ma (Fig. 6), similar to zircon Hf isotopes from the world-famous Koktokay No. 3 pegmatite ($\varepsilon_{Hf}(t) = +1.25$ to +2.39, $T_{DM} = 1102$ to 1174 Ma), close to CHUR but markedly deviated from the DM line (Fig. 7), indicating that magmas originated from two-end mixtures (older crust and mantle components). The Mesozoic Aral porphyritic granite has been dated at ~251 Ma (Rb–Sr isochron, Liu, 1993; K–Ar isochron for biotite, Liu et al., 1997), 210–220 Ma (SHRIMP zircon U–Pb, Wang et al., 2007, 2008) and

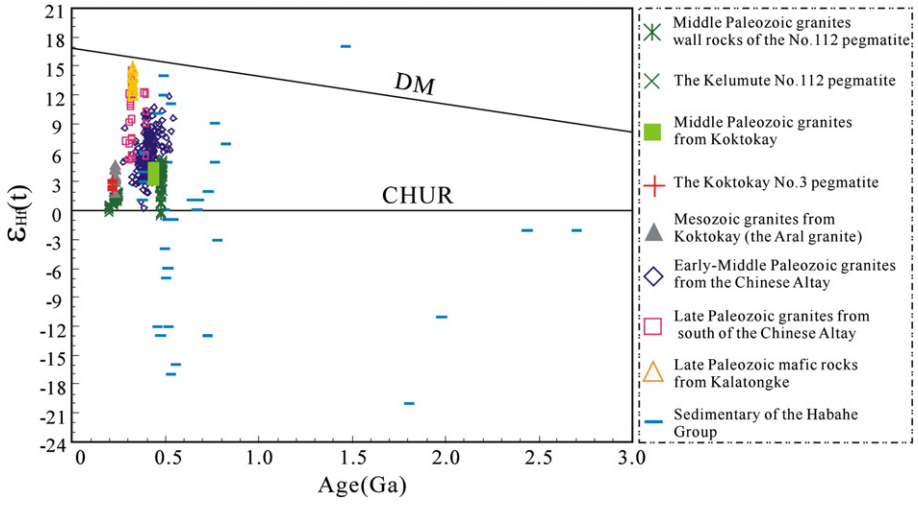

Fig. 7. Comparison diagram of $\varepsilon_{Hf}(t)$-age for zircons of mafic, granitc, pegmatitic and sedimentary rocks from the Chinese Altay. Data sources: Late Paleozoic mafic rocks (Zhang et al., 2009); Early–Middle Paleozoic granites (Cai et al., 2011a); Middle Paleozoic granites, the Aral granite and the No.3 pegmatite (Chen, 2011); Late Paleozoic granites (Tong, 2006); Sedimentary rocks (Long et al., 2007) and this study. Some data (Tong, 2006; Zhang et al., 2009) are obtained by the formula: $\varepsilon_{Hf} = 1.36\varepsilon_{Nd} + 2.95$ (Vervoort et al., 1999).

~233 Ma (LA-ICPMS zircon U–Pb, Chen, 2011) in different ways. As a potential parental granite for the Koktokay No. 3 pegmatite (Chen, 2011) and the largest of the three known Mesozoic granites (Aral granite, Jiangjunshan granite, and Shangkelan granite, Fig. 1) in the Chinese Altay (He et al., 1994) to date, it also shows lower positive $\varepsilon_{Hf}(t)$ values (+1 to +4), and older T_{DM} model ages (1007 to 1196 Ma) in zircons (Chen, 2011; Wang et al., 2007; Zhu et al., 2006). The gneissic biotite granite, widely distributed across the Koktokay mining area with an intrusion age of 410 Ma (Chen, 2011), has lower positive $\varepsilon_{Hf}(t)$ values (+2.2 to +3.7) and older T_{DM} model ages (1164 to 1256 Ma). Obviously, similar to the Paleozoic granites mentioned above, the Mesozoic igneous rock in the Chinese Altay, whether pegmatite or granite, is characterized by lower positive $\varepsilon_{Hf}(t)$ and older T_{DM} model ages in zircons, indicating that it originated from a common source area (Fig. 6).

Partial melting of mixed sources may be a common feature in NW China and the CAOB. Some of the Permo-Triassic intraplate magmatic activity and associated metallogeny in Central Asia and NW China is relevant to strike-slip activity, which is triggered either by the activity of a mantle plume or by upwelling asthenospheric melts (Pirajno, 2010). In fact, voluminous Late Paleozoic (320 to 250 Ma) calc-alkaline and alkaline granites occur along the strike-slip Irtysh Fault in the Chinese Altay (Tong, 2006). It has been suggested that mantle plumes of Tarim and Siberian were activated in 280 and 250 Ma, respectively, and directly resulted in the formation of large-scale ore deposits such as Ni–Cu–PGE, Cu–Mo, Fe–Pt, Au–Hg in the CAOB (Borisenko et al., 2006; Dobretsov et al., 2010; Pirajno, 2010; Pirajno et al., 2009). Normally, magmatic activity associated with mantle plumes, large igneous formations and lithosphere-scale strike-slip movements are involved in a great quantity of juvenile mantle-derived magma, showing larger positive εHf(t) values and younger T_{DM} model ages in their zircons (Sun et al., 2008).

Lower positive $\varepsilon_{Hf}(t)$ values and older T_{DM} model age in zircons from the Aral granites, Koktokay No. 3 and Kelumute No. 112 pegmatites, signify a mixture of older crust- and mantle-derived components; there was very little contribution of juvenile mantle-derived magma to Mesozoic magma activity in the Chinese Altay. Therefore, a petrogenetic model of the studied peraluminous granites and pegmatites, which resulted from decompression melting of thickened immature lower crust under post-collisional extensional setting, is put forward in this study.

5.4. Implications for tectonic evolution of CAOB in the Mesozoic era

Previous studies indicate that ore-bearing pegmatites can be formed at different stages during the continental evolutionary process, but metallization of rare metals may be concentrated in one or several stages (Aurisicchio et al., 2001; Morteani et al., 2000; Partington et al., 1995). In recent years, geochronological studies on pegmatites from the Chinese Altay show that rare metal-mineralized pegmatites formed mainly in the Mesozoic. The rim zone of the only superlarge-scale rare-metal ore deposit in Altay, the Koktokay No. 3 pegmatite, has been dated at 218.4 ± 5.8 Ma using isochron Rb–Sr (Zhu et al., 2006). Zircon SHRIMP U–Pb ages from zones I, V and VII were 220 ± 9 Ma, 198 ± 7 Ma and 213 ± 6 Ma, respectively (Wang et al., 2007). Zircon LA-ICPMS U–Pb ages from zones II, IV and VI of the cupola-shaped part, as well as from the fine-grained zone of the plate-shaped part of No. 3 pegmatite were dated at 211.9 ± 3.2 Ma, 214.9 ± 2.1 Ma, 212 ± 4.1 Ma and 212.0 ± 1.8 Ma, respectively (Chen, 2011). Zircon U–Pb ages of the Kelumute No. 112 pegmatite in this study ranged from 238.3 ± 2.0 to 210.7 ± 1.6 Ma. In addition, $^{40}Ar/^{39}Ar$ plateau ages of muscovite from Dakalasu Li–Be–Nb–Ta deposits and Xiaokalasu Nb–Ta deposits were dated at 248.42 ± 2.11 Ma and 233.79 ± 0.41 Ma, respectively (Wang et al., 2003b), and zircon LA-ICPMS U–Pb ages from some medium-scale Be–Nb–Ta deposits in Altay, such as Qunku, Jiamukai, Abagong–Talate and Amusitai pegmatites were dated at 207.2 ± 1.6, 212.2 ± 1.7, 246.8 ± 1.2 and 275.5 ± 4.2 Ma, respectively. All of the rare-metal pegmatites mentioned above were formed in the Permian and Triassic. Moreover, tens of pegmatites and wall rock granites have been selected to determine zircon Hf isotope composition, and the results indicate that all originated from a common source, with a gradual decrease in $\varepsilon_{Hf}(t)$ values from +4–+5 for the middle Ordovician and Silurian granites (wall rocks of pegmatites, 456 to 411 Ma) and to 0–+2.35 for the Triassic pegmatite (240 to 212 Ma) (unpublished data). These data likely indicate a gradual decrease in asthenospheric mantle activity from the synorogenic to postorogenic stage.

At present, basalts and granites are widely used in classification of tectonic settings and tracing of geotectonic evolution history, but studies of pegmatite to trace geotectonic evolution are very limited. As discussed above, we conclude that the Kelumute No. 112 pegmatite, like the Koktokay No. 3 and Aral granite, derived from partial melting of ancient crust with mantle-derived residual materials under a post-collision extensional setting. Pegmatite with Li–Be–Nb–Ta–Cs mineralization is classified as LCT-family pegmatite, which is characterized as peraluminous, enriched in B, Be, Li, P and alkalis (Na, K), and poor in Fe, Mg, and Ca, indicating a origin from partial melting of sedimentary pelites. Previous studies have shown that pelites, especially claystones related to evaporites, are richest in tourmalines, which provide abundant boron (Grew, 1996; Leeman and Sisson, 1996) and other components, such as Na, K, Li, Cl, F, P, Fe and Mn (Slack et al., 1989; Williams and McKibben, 1989). LCT-family pegmatites were commonly derived from peraluminous S-type granite under syn-orogenic or post-orogenic settings (Černý, 1991). It was reported that strong peraluminous granites mainly originated from post-collision tectonic settings and were formed by tectonic decompression melting after crustal thickening resulting from the orogeny process (Sylvester, 1998). Moreover, S-type peraluminous granites do exist in the Chinese Altay, but most are small granitic plutons that intruded in the Mesozoic era and formed under a post-orogenic setting (Wang et al., 2010). Therefore, we hypothesize that subduction of the paleo-Asian ocean crust did not terminate in the Late Permian. On the contrary, block amalgamation and collisional orogeny may have continued into the Triassic. This is consistent with the groundbreaking origin reported by very few scholars (Briggs et al., 2007; Xiao et al., 2006, 2008b, 2009). From the Late Paleozoic to Mesozoic, tectonic setting of the Chinese Altay changed from compression to extension, leading to decompression melting of thickening crust material and ultimately giving rise to the formation of peraluminous S-type granites and affinitive pegmatite magma. Therefore, our data and tectonic setting interpretations are of key significance to reconcile the controversy with respect to closure time of the Paleo-Asian Ocean and to present a better understanding of the accretionary tectonics of the southern CAOB during the Mesozoic era.

6. Conclusions

(1) The Kelumute No. 112 pegmatite in the Chinese Altay was mainly formed from 238.3 ± 2.0 to 210.7 ± 1.6 Ma, and the wall rocks of the Jideke two-mica granite and biotite granite are dated at 445.6 ± 4.3 and 455.6 ± 5.4 Ma, respectively, indicating no genetic relationship between the pegmatite and wall rocks.

(2) The Kelumute No. 112 pegmatite underwent a long-term evolutionary process with three stages: magmatic, magmatic–hydrothermal transition and hydrothermal stages, with durations of ~5 Ma, ~23 Ma and ~22 Ma, respectively.

(3) Parental magmas of the Kelumute No. 112 pegmatite and its wall rocks of Jideke two-mica granite and biotite granite originated from a common source, but result from distinct melting processes of immature crust under different tectonic settings.

(4) The Kelumute No. 112 pegmatite and Koktokay No. 3 pegmatite were created by crust thickening and decompression melting in a post-collision tectonic setting. Thus,

subduction of the paleo-Asian ocean crust did not terminate in the Late Permian. Block amalgamation and collisional orogeny may have continued into the Triassic.

Acknowledgments

Many thanks to engineer Xiangchen Zhang for his help during the field investigation and to Xiaoming Liu and Honglin Yuan for their help in the determination of zircon U – Pb age using LA-ICPMS. We also thank Hongfeng Tang for his help in the determining zircon Hf isotopic composition by LA-MC-ICPMS. We thank Prof. Chao Yuan for his constructive suggestions. Prof. Yun Liu, Drs. Yang and Song are thanked for their help with editing the manuscript. Editor-in-chief Nelson Eby, Prof. Wenjiao Xiao and another anonymous reviewer are sincerely thanked for their patience and constructive comments. This study was jointly supported by the National Basic Research Program of China (973 Program) (No. 2007CB411303), the National Supporting Program of China (305 Program) (No. 2007BAB25B01), and the National Science Foundation of China under Grants 41073051 and 40673052.

References

Andersen, T., 2002. Correction of common Pb in U – Pb analyses that do not report ^{204}Pb. Chemical Geology 192, 59–79.

Aurisicchio, C., Vito, C.D., Ferrini, V., Orlandi, P., 2001. Nb – Ta oxide minerals from miarolitic pegmatites of the Baveno pink granite, NW Italy. Mineralogical Magazine 65, 509–522.

Blichert-Toft, J., Albarède, F., 1997. The Lu – Hf geochemistry of the chondrites and the evolution of the mantle–crust system. Earth and Planetary Science Letters 148, 243–258.

Borisenko, A.S., Sotnikov, V.I., Izokh, A.E., Polyakov, G.V., Obolensky, A.A., 2006. Permo-Triassic mineralization in Asia and its relation to plume magmatism. Russian Geology and Geophysics 47, 170–186.

Briggs, S.M., Yin, A., Manning, C.E., Chen, Z.L., Wang, X.F., Grove, M., 2007. Late Paleozoic tectonic history of the Ertix Fault in the Chinese Altai and its implications for the development of the Central Asian Orogenic System. Geological Society of America Bulletin 119, 944–960.

Burnham, C.W., Ohmoto, H., 1980. Late stage processes of felsic magmatism. Mining Geology Special Issue 8, 1–11.

Buslov, M.M., Saphonova, I.Y., Watanabe, T., Obut, O.T., Fujiwara, Y., Iwata, K., Semakov, N.N., Sugai, Y., Smirnova, L.V., Kazansky, A.Y., 2001. Evolution of the Paleo-Asian Ocean (Altai-Sayan Region, Central Asia) and collision of possible Gondwana-derived terranes with the southern marginal part of the Siberian continent. Geosciences Journal 5, 203–224.

Buslov, M.M., Watanabe, T., Fujiwara, Y., Iwata, K., Smirnova, L.V., Yu Safonova, I., Semakov, N.N., Kiryanova, A.P., 2004. Late Paleozoic faults of the Altai region, Central Asia: tectonic pattern and model of formation. Journal of Asian Earth Sciences 23, 655–671.

Cai, K.D., Sun, M., Yuan, C., Zhao, G.C., Xiao, W.J., Long, X.P., Wu, F.Y., 2011a. Geochronology, petrogenesis and tectonic significance of peraluminous granites from the Chinese Altai, NW China. Lithos 127, 261–281.

Cai, K.D., Sun, M., Yuan, C., Long, X.P., Xiao, W.J., 2011b. Geological framework and Paleozoic tectonic history of the Chinese Altai, NW China: a review. Russian Geology and Geophysics 52, 1619–1633.

Cai, K.D., Sun, M., Yuan, C., Zhao, G.C., Xiao, W.J., Long, X.P., Wu, F.Y., 2011c. Prolonged magmatism, juvenile nature and tectonic evolution of the Chinese Altai, NW China: evidence from zircon U – Pb and Hf isotopic study of Paleozoic granitoids. Journal of Asian Earth Sciences 42, 949–968.

Černý, P., 1991. Fertile granites of Precambrian rare-element pegmatite fields: is geochemistry controlled by tectonic setting or source lithologies. Precambrian Research 51, 429–468.

Černý, P., Erict, T.S., 2005. The classification of granitic pegmatites revisited. The Canadian Mineralogist 43, 2005–2026.

Chen, J.F., 2011. Geochemistry of the plate part in Altai No. 3 pegmatite and its formation and evolution. A dissertation submitted to graduate university of Chinese Academy of Sciences for the degree of Master of Philosophy, pp. 1–86 (in Chinese with English abstract).

Chen, J.F., Han, B.F., Ji, J.Q., Zhang, L., Xu, Z., He, G.Q., Wang, T., 2010. Zircon U-Pb ages and tectonic implications of Paleozoic plutons in northern West Junggar, North Xinjiang, China. Lithos 115, 137–152.

Chen, F.W., Li, H.Q., Wang, D.H., Cai, H., Chen, W., 1999. New chronological evidence for Yanshanian diagenetic mineralization in China's Altay orogenic belt. Chinese Science Bulletin 44, 1142–1148 (in Chinese with English abstract).

Coleman, R., 1989. Continental growth of Northwest China. Tectonics 8, 621–635.

Dobretsov, N.L., Borisenko, A.S., Izokh, A.E., Zhmodik, S.M., 2010. A thermochemical model of Eurasian Permo-Triassic mantle plumes as a basis for prediction and exploration for Cu – Ni – PGE and rare-metal ore deposits. Russian Geology and Geophysics 51, 903–924.

Filippova, I.B., Bush, V.A., Didenko, A.N., 2001. Middle Paleozoic subduction belts: the leading factor in the formation of the Central Asian fold-and-thrust belt. Russian Journal of Earth Sciences 3, 405–426.

Fuertes-Fuente, M., Martin-izard, A., Boiron, M.C., Viñuela, M., 2000. P–T path and fluid evolution in the Franqueira granitic pegmatite, Central Galicia, Northwestern Spain. The Canadian Mineralogist 38, 1163–1175.

Grew, E.S., 1996. Borosilicates (exclusive of tourmaline) and boron in rock forming minerals in metamorphic environments. In: Grew, E.S., Anovitz, L.M. (Eds.), Boron: Mineralogy, Petrology and GeochemistryReviews in Mineralogy and Geochemistry 33, 387–502.

Griffin, W.L., Wang, X., Jackson, S.E., Pearson, N.J., O'Reilly, S.Y., Xu, X.S., Zhou, X.M., 2002. Zircon chemistry and magma mixing, SE China: in-situ analysis of Hf isotopes, Tonglu and Pingtan igneous complexes. Lithos 61, 237–269.

Han, B.F., Guo, Z.J., Zhang, Z.C., Zhang, L., Chen, J.F., Song, B., 2010. Age, geochemistry, and tectonic implications of a late Paleozoic stitching pluton in the North Tian Shan suture zone, western China. Geological Society of American Bulletin 122, 627–640.

Han, B.F., He, G.Q., Wang, X.C., Guo, Z.J., 2011. Late Carboniferous collision between the Tarim and Kazakhstan–Yili terranes in the western segment of the South Tian Shan Orogen, Central Asia, and implications for the Northern Xinjiang, western China. Earth-Science Reviews 109, 74–93.

He, G.Q., Han, B.F., Yue, Y.J., Wang, J.H., 1990. Tectonic division and crustal evolution of Altay orogenic belt in China. Geoscience of Xinjiang 2, 9–20 (in Chinese with English abstract).

He, G.Q., Li, M.S., Liu, D.Q., 1994. Paleozoic crustal evolution and mineralization in Xinjiang of China. Urumqi: Xinjiang People's Publishing House, Hong Kong: Culture and Education Press of Hong Kong, pp. 1–437 (in Chinese).

Hendrix, M.S., Graham, S.A., Amory, J.Y., Badarch, G., 1996. Noyon Uul Syncline, southern Mongolia; lower Mesozoic sedimentary record of the tectonic amalgamation of Central Asia. Geological Society of America Bullutin 108, 1256–1274.

Hoskin, P.W.O., 2005. Trace element composition of hydrothermal zircon and the alteration of Hadean zircon from the Jack Hills, Australia. Geochimica et Cosmochimica Acta 69, 637–648.

Hu, A.Q., Jahn, B.M., Zhang, G.X., Chen, Y.B., Zhang, Q.F., 2000. Crustal evolution and Phanerozoic crustal growth in northern Xinjiang: Nd isotopic evidence. Part I: Isotopic characterization of basement rocks. Tectonophysics 328, 15–51.

Hu, F.F., Fan, H.R., Yang, J.H., Wan, Y.S., Liu, D.Y., Zhai, M.G., Jin, C.W., 2004. Mineralizing age of the Rushan lode gold deposit in the Jiaodong Peninsula: SHRIMP U – Pb dating on hydrothermal zircon. Chinese Science Bulletin 49, 1629–1636.

Jolliff, B.L., Papike, J.J., Shearer, C.K., 1992. Petrogenetic relationships between pegmatite and granite based on geochemistry of muscovite in pegmatite wall zones, Black Hills, South Dkota, USA. Geochimica et Cosmochimica Acta 56, 1915–1939.

Kheraskova, T.N., Didenko, A.N., Bush, V.A., Volozh, Y.A., 2003. The Vendian–Early Paleozoic history of the continental margin of Eastern Paleogondwana, Paleoasian Ocean, and Central Asian Foldbelt. Russian Journal of Earth Sciences 5, 165–184.

Kröner, A., Windley, B.F., Badarch, G., Tomurtogoo, O., Hegner, E., Jahn, B.M., Gruschka, S., Khain, E.V., Demoux, A., Wingate, M.T.D., 2007. Accretionary growth and crust-formation in the Central Asian Orogenic Belt and comparison with the Arabian–Nubian shield. Geological Society of America 200, 181–209.

Leeman, W.P., Sisson, V.B., 1996. Geochemistry of boron and its implications for crustal and mantle processes. In: Grew, E.S., Anovitz, L.M. (Eds.), Boron: Mineralogy, Petrology and GeochemistryReviews In Mineralogy and Geochemistry 33, 645–707.

Li, J.Y., Xiao, W.J., Wang, K.Z., Sun, G.H., Gao, L.M., 2003. Neoproterozoic–Paleozoic tectonostratigraphy, magmatic activities and tectonic evolution of the eastern Xinjiang, NW China. In: Jingwen, Mao, Goldfarb, Seltman, Wang, Xiao, Hart (Eds.), Tectonic evolution and Metallogeny of the Chinese Altai and Tianshan. IAGOD Guidebook Series, 10. CERCAM /NHM, London, pp. 31–74.

Li, H.J., He, G.Q., Wu, T.R., Wu, B., 2006. Confirmation of Altai–Mongolia microcontinent and its implications. Acta Petrologica Sinica 22, 1369–1379 (in Chinese with English abstract).

Li, T.D., Qi, Z.M., Xiao, S.L. Wu, B.Q., 1996. New improvement of comparative study of geology and mineralization of Altai between China and Kazakhstan. In: Chinese Geological Society (Ed.) Thesis Volume of the Symposium of the 8th Five Year Plan of Geoscience for Contribution to 30th IGC. Metallurgical Industrial Publishing House, Beijing, 256–259 (in Chinese).

Liu, W., 1993. Whole-rock isochron ages of plutons, crustal movements and evolution of tectonic setting in the Altay Mts., Xinjiang Uygur Autonomous Region. Geosciences of Xinjiang, No. 4. Geological Press, Beijing, pp. 35–50 (in Chinese).

Liu, W., Liu, C.Q., Masuda, A., 1997. Complex trace-element effects of mixing-fractional crystallization composite processes: applications to the Alaer granite pluton, Altay Mountains, Xinjiang, Northwestern China. Chemical Geology 135, 103–124.

Liu, F., Li, Y.H., Mao, J.W., Yang, F.Q., 2008a. SHRIMP U – Pb ages of the Abagong granites in the Altay Orogen and their geological implications. Acta Geoscientica Sinica 29, 795–804 (in Chinese with English abstract).

Liu, Y.S., Hu, Z.C., Gao, S., Günther, D., Xu, J., Gao, C.G., Chen, H.H., 2008b. In situ analysis of major and trace elements of anhydrous minerals by LA-ICP-MS without applying an internal standard. Chemical Geology 257, 34–43.

Liu, Y.S., Gao, S., Hu, Z.C., Gao, C.G., Zong, K.Q., Wang, D.B., 2010. Continental and oceanic crust recycling-induced melt–peridotite interactions in the Trans-North China Orogen: U – Pb dating, Hf isotopes and trace elements in zircon from mantle xenoliths. Journal of Petrology 51, 537–571.

London, D., 1986. The magmatic–hydrothermal transition in the Tanco rare-element pegmatite: evidence from fluid inclusions and phase equilibrium experiments. American Mineralogist 71, 376–395.

London, D., 2005. Granitic pegmatites: an assessment of current concepts and directions for the future. Lithos 80, 281–303.
London, D., Černý, P., Loomis, J.L., Pan, J.J., 1990. Phosphorus in alkali feldspars of rare-element granitic pegmatites. The Canadian Mineralogist 28, 771–786.
Long, X.P., Sun, M., Yuan, C., Xiao, W.J., Lin, S.F., Wu, F.Y., Xia, X.P., Cai, K.D., 2007. U–Pb and Hf isotopic study of zircons from metasedimentary rocks in the Chinese Altai: implications for Early Paleozoic tectonic evolution. Tectonics TC5015. http://dx.doi.org/10.1029/2007TC002128.
Long, X.P., Sun, M., Yuan, C., Xiao, W.J., Cai, K.D., 2008. Early Paleozoic sedimentary record of the Chinese Altai: implications for its tectonic evolution. Sedimentary Geology 208, 88–100.
Long, X.P., Yuan, C., Sun, M., Xiao, W.J., Zhao, G.C., Wang, Y.J., Cai, K.D., 2010. Detrital zircon ages and Hf isotopes of the early Paleozoic Flysch sequence in the Chinese Altai, NW China: new constraints on depositional age, provenance and tectonic evolution. Tectonophysics 480, 213–231.
Lu, H.Z., Wang, Z.G., Li, Y.S., 1996. Magma/fluid transition and genesis of pegmatite dike No. 3 at Altay, Xinjiang. Acta Mineralogica Sinica 16, 1–7 (in Chinese).
Ludwig, K.R., 2003. User's manual for Isoplot/Ex, Version 3. 00. A Geochronological Toolkit for Microsoft Excel. Berkeley Geochronology Center Special Publication 4, 1–70.
Morgan VI, G.B., London, D., 1999. Crystallization of the little three layered pegmatite–aplite dike, Ramona District, California. Contributions to Mineralogy and Petrology 136, 310–330.
Morteani, G., Preinfalk, C., Horn, A., 2000. Classification and mineralization potential of the pegmatites of the Eastern Brazilian Province. Mineralium Deposita 35, 638–655.
Partington, G.A., McNaughton, N.J., Willims, I.S., 1995. A review of the geology, mineralization, and geochronology of the Greenbushes pegmatite, Western Australia. Economic Geology 90, 616–635.
Pirajno, F., 2010. Intracontinental strike-slip faults, associated magmatism, mineral systems and mantle dynamics: examples from NW China and Altay-Sayan (Siberia). Journal of Geodynamics 50, 325–346.
Pirajno, F., Ernst, R.E., Borisenko, A.S., Fedoseev, G., Naumov, E.A., 2009. Intraplate magmatism in Central Asia and China and associated metallogeny. Ore Geology Reviews 35, 114–136.
Ren, B.Q., Zhang, H., Tang, Y., Lv, Z.H., 2011. LA-ICPMS U–Pb zircon geochronology of the Altai pegmatites and its geological significance. Acta Mineralogica Sinica 31, 587–596.
Safonova, I.Y., Buslov, M.M., Iwata, K., Kokh, D.A., 2004. Fragments of Vendian–Early Carboniferous oceanic crust of the Paleo-Asian Ocean in foldbelts of the Altai-Sayan region of Central Asia: geochemistry, biostratigraphy and structural setting. Gondwana Research 7, 771–790.
Slack, J.F., Palmer, M.R., Stevens, B.P.J., 1989. Boron isotope evidence for the involvement of non-marine evaporites in the origin of the Broken Hill ore deposits. Nature 342, 913–916.
Soderlund, U., Patchett, P.J., Vervoort, J.D., Isachsen, C.E., 2004. The ^{176}Lu decay constant determined by Lu–Hf and U–Pb isotope systematics of Precambrian mafic intrusions. Earth and Planetary Sciences Letters 219, 311–324.
Sun, M., Yuan, C., Xiao, W.J., Long, X.P., Xia, X.P., Zhao, G.C., Lin, S.F., Wu, F.Y., Kroner, A., 2008. Zircon U–Pb and Hf isotopic study of gneissic rocks from the Chinese Altai: progressive accretionary history in the early to middle Palaeozoic. Chemical Geology 247, 352–383.
Sylvester, P.J., 1998. Post-collisional strongly peraluminous granites. Lithos 45, 29–44.
Tang, J.H., Gu, L.X., Zhang, Z.Z., Wu, C.Z., San, J.Z., Wang, C.S., Liu, S.H., Zhang, G.H., 2008. Characteristics, age and origin of the Xianshuiquan gneissose granites in eastern Tianshan. Acta Petrologica Sinica 23, 1830–1840 (in Chinese with English abstract).
Tong, Y., 2006. Geochronology, origin of the Late Paleozoic granitoids from the Altai Orogen in China and their geological significance. Beijing: A Dissertation Submitted to Chinese Academy of Geological Sciences for the Degree of Doctor of Philosophy, pp. 1–112 (in Chinese with English abstract).
Tong, Y., Wang, T., Hong, D.W., Liu, X.M., Han, B.F., 2005. Zircon U–Pb age of syn-orogenic Tielieke pluton in the western part of Altay orogenic belt and its structural implications (Sup.) Acta Geoscientica Sinica 26, 74–77 (in Chinese with English abstract).
Tong, Y., Wang, T., Kovach, Hong, D.W., Han, B.F., 2006a. Age and origin of the Takeshiken postorogenic alkali-rich intrusive rocks in southern Altai, near the Mongolian border in China and its implications for continental growth. Acta Petrologica Sinica 22, 1267–1278 (in Chinese with English abstract).
Tong, Y., Hong, D.W., Wang, T., Wang, S.G., Han, B.F., 2006b. TIMS U–Pb zircon ages of Fuyun post-orogenic linear granite plutons on the southern margin of Altay orogenic belt and their implications. Acta Petrologica et Mineralogica 25, 85–89 (in Chinese with English abstract).
Tong, Y., Wang, T., Hong, D.W., Dai, Y.J., 2007. Ages and origin of early Devonian granites from the north part of Chinese Altai Mountains and its tectonic implications. Acta Petrologica Sinica 23, 1933–1944 (in Chinese with English abstract).
Tong, Y., Wang, T., Siebel, W., Hong, D.W., Sun, M., 2012. Recognition of early Carboniferous alkaline granite in the southern Altai orogen: post-orogenic processes constrained by U–Pb zircon ages, Nd isotopes, and geochemical data. International Journal of Earth Sciences 101, 937–950.
Vervoort, J.D., Patchett, P.J., Blichert-Toft, J., Albarède, F., 1999. Relationships between Lu–Hf and Sm–Nd isotopic systems in the global sedimentary system. Earth and Planetary Science Letters 168, 79–99.
Wang, X.J., Zou, T.R., 1981. Study of Pegmatite Minerals of the Altay Region. Scientific Publishing House, Beijing, pp. 1–78 (in Chinese).
Wang, D.H., Chen, Y.C., Zou, T.R., Xu, Z.G., Li, H.Q., Chen, W., Chen, F.W., Tian, F., 2000. ^{40}Ar/^{39}Ar dating for the Azubai rare metal-gem deposit in Altay, Xinjiang: New evidence for Yanshanian mineralization of rare metals. Geological Review 46, 307–311 (in Chinese).
Wang, D.H., Chen, Y.C., Xu, Z.G., 2002. Metallogenetic Series and Regularity of the Altay Metallogenic Province. Atomic Energy Press, Beijing, pp. 1–493 (in Chinese).
Wang, Y.X., Mooney, W.D., Yuan, X.C., Coleman, R.G., 2003a. The crustal structure from the Altai Mountains to the Altyn Tagh fault, northwest China. Journal of Geophysical Research 108, 2322–2339.
Wang, D.H., Chen, Y.C., Xu, Z.G., 2003b. ^{40}Ar/^{39}Ar isotope dating on muscovites from Indosinian rare-metal deposits in Central Altay, Northwestern China. Bulletin of Mineralogy Petrology and Geochemistry 22, 14–17 (in Chinese with English abstract).
Wang, J.B., Wang, Y.W., Wang, L.J., 2004a. The Junggar immature continental crust province and its mineralization. Acta Geologica Sinica 78, 337–344.
Wang, D.H., Zou, T.R., Xu, Z.G., Yu, J.J., 2004b. Advance in the study of using pegmatite deposits as the tracer of orogenic process. Advances in earth science 19, 614–620 (in Chinese with English abstract).
Wang, T., Hong, D.W., Tong, Y., Han, B.F., Shi, Y.R., 2005. Zircon U–Pb SHRIMP age and origin of post-orogenic Lamazhao granitic pluton from Altai orogen: its implications for vertical continental growth. Acta Petrologica Sinica 21, 640–650 (in Chinese with English abstract).
Wang, T., Hong, D.W., Jahn, B.M., Tong, Y., 2006. Timing, petrogenesis, and setting of Paleozoic synorogenic intrusions from the Altai Mountains, Northwest China: implications for the tectonic evolution of an accretionary orogen. Journal of Geology 114, 735–751.
Wang, T., Tong, Y., Jahn, B.M., Zou, T.R., Wang, Y.B., Hong, D.W., Han, B.F., 2007. SHRIMP U–Pb Zircon geochronology of the Altai No. 3 Pegmatite, NW China, and its implications for the origin and tectonic setting of the pegmatite. Ore Geology Reviews 32, 325–336.
Wang, T., Jahn, B.M., Kovach, V.P., Tong, Y., 2008. Mesozoic anorogenic granitic magmatism in the Altai Paleozoic accretionary orogen, NW China, and its implications for crustal architecture and growth AOGS 5th Annual General Meeting. Korea, Busan.
Wang, T., Jahn, B.M., Kovach, V.P., Tong, Y., Hong, D.W., Han, B.F., 2009. Nd–Sr isotopic mapping of the Chinese Altai and implications for continental growth in the Central Asian Orogenic Belt. Lithos 110, 359–372.
Wang, T., Tong, Y., Li, S., Zhang, J.J., Shi, X.J., Li, J.Y., Han, B.F., 2010. Spatial and temporal variations of granitoids in the Altay orogen and their implications for tectonic setting and crustal growth: perspectives from Chinese Altay. Acta Petrologica et Mineralogica 29, 595–618 (in Chinese with English abstract).
Webster, J.D., Thomas, R., Rhede, D., Förster, H.J., Seltmann, R., 1997. Melt inclusions in quartz from an evolved peraluminous pegmatite: geochemical evidence for strong tin enrichment in flourine-rich and phosphorus-rich residual liquids. Geochimica et Cosmochimica Acta 61, 2589–2604.
Williams, A.E., McKibben, M.A., 1989. A brine interface in the Salton Sea Geothermal System, California: fluid geochemical and isotopic characteristics. Geochimica et Cosmochimica Acta 53, 1905–1920.
Windley, B.F., Kroener, A., Guo, J., Qu, G., Li, Y., Zhang, C., 2002. Neoproterozoic to Paleozoic geology of the Altai Orogen, NW China: new zircon age data and tectonic evolution. Journal of Geology 110, 719–737.
Windley, B.F., Alexeiev, D., Xiao, W.J., Kröner, A., Badarch, G., 2007. Tectonic models for accretion of the Central Asian Orogenic Belt. Journal of the Geological Society 164, 31–47.
Woodhead, J., Hergt, J., Shelley, M., Eggins, S., Kemp, R., 2004. Zircon Hf-isotope analysis with an excimer laser, depth profiling, ablation of complex geometries, and concomitant age estimation. Chemical Geology 209, 121–135.
Wu, Y.B., Zheng, Y.F., 2004. Genesis of zircon and its constraints on interpretation of U–Pb age. Chinese Science Bulletin 49, 1554–1569.
Wu, C.N., Zhu, J.C., 1995. Study of compositions of melting fluid inclusions in pegmatite, Altay, Xinjiang. Geochimica 24, 351–358 (in Chinese with English abstract).
Wu, B.Q., Zou, T.R., 1989. The genesis of granitic pegmatites in Xinjiang Altai. Mineral and Geology of Xinjiang 1, 60–70 (in Chinese).
Wu, C.N., Zhu, J.C., Liu, C.S., 1994. A study on the inclusions in spodumenes from Altai pegmatite. Xinjiang. Geotectonica et Metallonenia 18, 353–362 (in Chinese with English abstract).
Wu, B., He, G.Q., Wu, T.R., Li, H.J., Luo, H.L., 2006. Discovery of the Buergen ophiolitic mélange belt in Xinjiang and its tectonic significance. Geology in China 33, 476–486 (in Chinese with English abstract).
Xiao, X.C., Tang, Y.Q., Feng, Y.M., Zhu, B.Q., Li, J.Y., Zhao, M., 1992. Tectonic Evolution of the Northern Xinjiang and its Adjacent Region. Geological Publishing House, Beijing, pp. 1–180 (in Chinese with English abstract).
Xiao, W.J., Windley, B.F., Badarch, G., Sun, S., Qin, K.Z., 2004. Paleozoic accretionary and convergent tectonics of the southern Altaids: implications for the growth of Central Asia. Journal of the Geological Society 161, 339–342.
Xiao, W.J., Han, C.M., Yuan, C., Chen, H.L., Sun, M., Lin, S.F., Li, Z.L., Mao, Q.G., Zhang, J.E., Sun, S., Li, J.L., 2006. Unique Carboniferous–Permian tectonic–metallogenic framework of Northern Xinjiang (NW China): constraints for the tectonics of the southern Paleoasian Domain. Acta Petrologica Sinica 22, 1062–1076 (in Chinese with English abstract).
Xiao, W.J., Pirajno, F., Seltmann, R., 2008a. Geodynamics and metallogeny of the Altaid orogen. Journal of Asian Earth Sciences 32, 77–81.
Xiao, W.J., Han, C.M., Yuan, C., Sun, M., Lin, S.F., Chen, H.L., Li, Z.L., Li, J.L., Sun, S., 2008b. Middle Cambrian to Permian subduction-related accretionary orogenesis of Northern Xinjiang, NW China: implications for the tectonic evolution of central Asia. Journal of Asian Earth Sciences 32, 102–117.
Xiao, W.J., Windley, B.F., Huang, B.C., Han, C.M., Yuan, C., Chen, H.L., Sun, M., Sun, S., Li, J.Y., 2009. End-Permian to mid-Triassic termination of the accretionary processes of the southern Altaids: implications for the geodynamic evolution, Phanerozoic continental growth, and metallogeny of Central Asia. International Journal of Earth Sciences 98, 1189–1217.

Xiao, W.J., Huang, B.C., Han, C.M., Sun, S., Li, J.L., 2010. A key to understanding the architecture of accretionary orogens. Gondwana Research 18, 253–273.
Xu, J.F., Chen, F.R., Yu, X.Y., Niu, H.C., Zheng, Z.P., 2001. Kuerti ophiolite in Altay Area of North Xinjiang: magmatism of an ancient back-arc basin. Acta Petrologica et Mineralogica 20, 244–352 (in Chinese with English abstract).
Xu, J., Chen, F., Yu, X., Niu, H., Zhen, Z., 2003. Kuerti ophiolite in Altay area of north Xinjiang: magmatism of an ancient back-arc basin. Acta Petrologica et Mineralogica 20, 344–352 (in Chinese with English abstract).
Yuan, C., Sun, M., Xiao, W.J., Li, X.H., 2006. Paleozoic accretion of Chinese Altai: geochronological constraints from granitoids. Abstract of Western Pacific Geophysics Meeting, Beijing, China.
Yuan, C., Sun, M., Xiao, W.J., Li, X.H., Chen, H.L., Lin, S.F., Xia, X.P., Long, X.P., 2007a. Accretionary orogenesis of the Chinese Altai: insights from Paleozoic granitoids. Chemical Geology 242, 22–39.
Yuan, H.L., Gao, S., Liu, X.M., Li, H.M., Günther, D., Wu, F.Y., 2007b. Accurate U–Pb age and trace element determinations of zircon by laser ablation-inductively coupled plasma mass spectrometry. Geoanalytical and Geostandard Research 28, 353–370.
Zhang, H., 2001. The geochemical behaviors and mechanisms of incompatible trace elements in the magmatic–hydrothermal transition system: a case study of Altay No. 3 pegmatite, Xinjiang. Guiyang: A Dissertation Submitted to Institute of Geochemistry for the Degree of Doctor of Philosophy, pp. 1–172 (in Chinese with English abstract).
Zhang, H., Liu, C.Q., 2001. Tetrad effect of REE in apatites from pegmatite No. 3, Altay, Xinjiang and its implications. Geochimica 30, 323–334 (in Chinese with English abstract).
Zhang, Q.F., Hu, A., Zhang, G.X., 1994. Evidence from isotopic age for presence of Mesozoic–Cenozoic magmatic activities in Altai region, Xinjiang. Geochimica 23, 269–280 (in Chinese with English abstract).
Zhang, J.H., Wang, J.B., Ding, R.F., 2000. Characteristics and U–Pb ages of zircon in metavolcanics from the Kangbutiebao Formation in the Altay region, Xinjiang. Regional Geology of China 19, 281–287 (in Chiese with English abstract).
Zhang, H.X., Niu, H.C., Terada, K., Yu, X.Y., Sato, H., Ito, J., 2003. Zircon SHRIMP U–Pb dating on plagiogranite from the Kuerti ophiolite in Altay, North Xinjiang. Chinese Science Bulletin 48, 2,231–2,235.
Zhang, A.C., Wang, R.C., Hu, H., Zhang, H., Zhu, J.C., Chen, X.M., 2004. The complex zonation of columbite-group minerals from the Koktokay No. 3 granitic pegmatite dyke, Altay, NW China and its petrological implications. Acta Geologica Sinica, 78, pp. 181–189 (in Chinese with English abstract).
Zhang, Z.C., Mao, J.W., Chai, F.M., Yan, S.H., Chen, B.L., 2009. Geochemistry of the Permian Kalatongke mafic intrusions, Northern Xinjiang, Northwest China: implications for the genesis of magmatic Ni–Cu sulfide deposits. Economic Geology 104, 185–203.
Zhu, Y.F., 2007. The Indo-China Movement and it's metallogeny of Xinjiang. Geological Bulletin of China 26, 510–518 (in Chinese with English abstract).
Zhu, Y.F., Song, B., 2006. Petrology and SHRIMP chronology of mylonitized Tianger granite, Xinjiang: also about the dating on hydrothermal zircon rim in granite. Acta Petrologica Sinica 22, 135–144 (in Chinese with English abstract).
Zhu, J.C., Wu, C.N., Liu, C.S., Li, F.C., 2000. Magmatic–hydrothermal evolution and genesis of Koktokay No. 3 rare metal pegmatite dyke, Altai, China. Geological Journal of China Universities 6, 40–52 (in Chinese with English abstract).
Zhu, Y.F., Zeng, Y.S., Gu, L.B., 2006. Geochemistry of the rare metal-bearing pegmatite No. 3 vein and related granites in the Keketuohai region, Altay Mountains, northwest China. Journal of Asian Earth Sciences 27, 61–77.
Zou, T.R., Zhang, X.C., Jia, F.Y., 1986. A discussion about contributing factor of the Altai No. 3 pegmatite. Mineral Deposits 5, 34–48 (in Chinese with English abstract).